HHS Public Access

Author manuscript

Cell Rep. Author manuscript; available in PMC 2023 June 19.

Published in final edited form as:

Cell Rep. 2023 May 30; 42(5): 112496. doi:10.1016/j.celrep.2023.112496.

HAPSTR1 localizes HUWE1 to the nucleus to limit stress signaling pathways

Julie K. Monda[1], **Xuezhen Ge**[1], **Moritz Hunkeler**[2,3], **Katherine A. Donovan**[2,3], **Michelle W. Ma**[2,3], **Cyrus Y. Jin**[2], **Marilyn Leonard**[1], **Eric S. Fischer**[2,3], **Eric J. Bennett**[1,4,*]

[1]School of Biological Sciences, Department of Cell and Developmental Biology, University of California, San Diego, La Jolla, CA 92093, USA

[2]Department of Cancer Biology, Dana-Farber Cancer Institute, Boston, MA 02215, USA

[3]Department of Biological Chemistry and Molecular Pharmacology, Harvard Medical School, Boston, MA 02115, USA

[4]Lead contact

SUMMARY

HUWE1 is a large, enigmatic HECT-domain ubiquitin ligase implicated in the regulation of diverse pathways, including DNA repair, apoptosis, and differentiation. How HUWE1 engages its structurally diverse substrates and how HUWE1 activity is regulated are unknown. Using unbiased quantitative proteomics, we find that HUWE1 targets substrates in a largely cell-type-specific manner. However, we identify C16orf72/HAPSTR1 as a robust HUWE1 substrate in multiple cell lines. Previously established physical and genetic interactions between HUWE1 and HAPSTR1 suggest that HAPSTR1 positively regulates HUWE1 function. Here, we show that HAPSTR1 is required for HUWE1 nuclear localization and nuclear substrate targeting. Nuclear HUWE1 is required for both cell proliferation and modulation of stress signaling pathways, including p53 and nuclear factor kB (NF-κB)-mediated signaling. Combined, our results define a role for HAPSTR1 in gating critical nuclear HUWE1 functions.

In brief

Monda et al. find that the substrates of the ubiquitin ligase, HUWE1, are diverse and largely cell-type specific. HAPSTR1 is a robust substrate of HUWE1 and is required for nuclear localization of HUWE1. Nuclear HUWE1 is required for cell proliferation and modulation of stress signaling pathways.

Graphical Abstract

*Correspondence: e1bennett@ucsd.edu.

AUTHOR CONTRIBUTIONS

Conceptualization, J.K.M., E.S.F., and E.J.B.; formal analysis, K.A.D., E.S.F., and E.J.B.; investigation, J.K.M., X.G., K.A.D., M.W.M., C.Y.J., M.L., and E.J.B.; resources, M.H.; writing – original draft, E.J.B.; writing – review and editing, J.K.M., M.H., E.S.F., and E.J.B.; visualization, J.K.M. and E.J.B.; supervision and funding acquisition, E.S.F. and E.J.B.

SUPPLEMENTAL INFORMATION

Supplemental information can be found online at https://doi.org/10.1016/j.celrep.2023.112496.

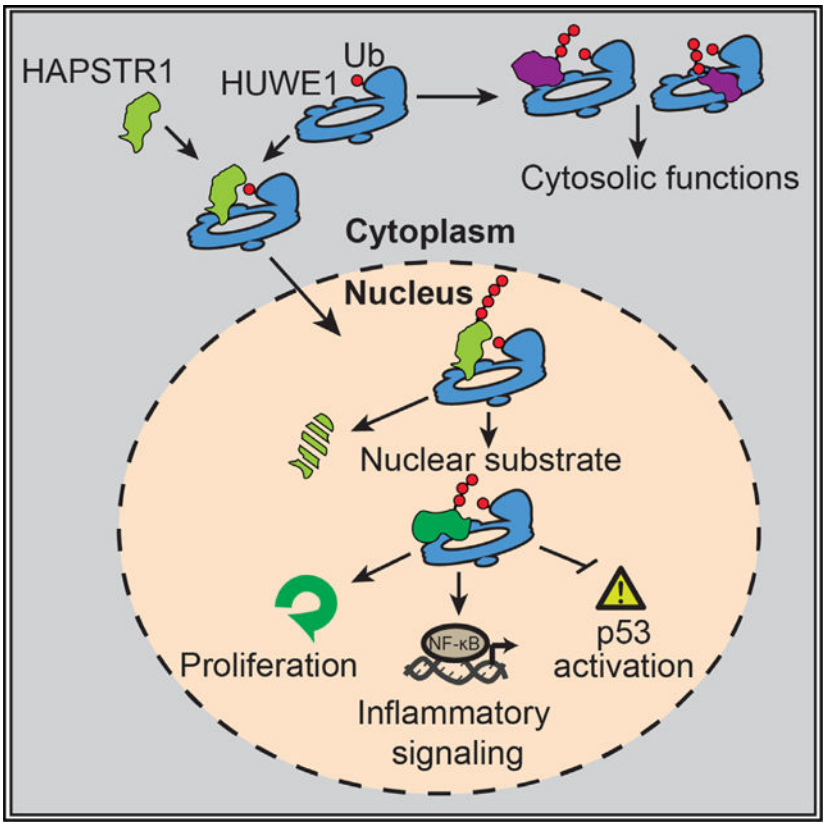

INTRODUCTION

Ubiquitin ligases directly engage substrates and provide specificity within the protein ubiquitylation cascade.[1,2] With over 600 putative ubiquitin ligases encoded within the human genome, a diversity of substrate-targeting mechanisms have been sdescribed.[2–4] Substrate ubiquitylation is often tightly regulated to prevent spurious targeting of substrates and ensure precise pathway regulation. Some ligases reportedly engage a highly diverse set of substrates with undefined mechanisms.[4–7] How these broadly acting ligases engage their substrates, and how these ligases are regulated remain open questions.

HUWE1 is one such enigmatic ubiquitin ligase that has many reported substrates regulating highly diverse cellular pathways.[7,8] HUWE1 is a giant and highly abundant HECT-domain ubiquitin ligase with a variety of protein interaction domains that have been shown to target specific substrates.[9–12] Recent structural characterization of full-length human HUWE1 revealed a solenoid architecture built by armadillo repeats to form a central cavity and the HECT domain positioned above the ring plane.[13] The characterized HUWE1 substrate, DDIT4,[14] was shown to bind to the inner armadillo repeats within HUWE1, suggesting a new mode of substrate interaction.[13] This type of plasticity with regard to substrate engagement may be desirable for a subset of ligases, such as quality-control ligases that need to target a diverse range of damaged or misfolded substrates. Indeed, HUWE1 has been shown to act in a quality-control manner to target orphan proteins of multi-subunit complexes for degradation.[15–18] However, how HUWE1 and similar ubiquitin ligases with

demonstrated substrate plasticity are regulated to prevent spurious substrate degradation is incompletely understood.

One mechanism that is employed to regulate ubiquitin ligase function is to restrict ligase subcellular localization. This feature is characteristic of ligases that regulate endoplasmic reticulum (ER) function.[19] HUWE1 is broadly localized to both the cytoplasm and the nucleoplasm and has many reported substrates within each compartment.[10,12,14,20–30] HUWE1 has been shown to regulate many nuclear processes, including transcription, DNA damage responses, and stress signaling. HUWE1 can ubiquitylate transcriptional regulators, such as c-Myc, N-Myc, and p53, to govern developmental and stress-dependent signaling pathways.[9,10,29–37] Further, HUWE1 regulates DNA damage responses by ubiquitylating diverse substrates ranging from histones to the DNA repair polymerase λ.[22,26,27,35,38,39] Human mutations within HUWE1 have been linked to intellectual disability disorders and neurodevelopmental defects, underscoring the broad role HUWE1 plays in regulating nuclear functions.[8,40–42]

To understand how HUWE1 can target diverse substrates in a controlled manner, we used an unbiased proteomic approach to systematically identify HUWE1 substrates. Nuclear localized proteins are enriched among the identified HUWE1 substrates, and we identify C16orf72/HUWE1-associated protein modifying stress responses (HAPSTR1) as a robust HUWE1 nuclear substrate. Despite being a substrate, HAPSTR1 has a strong positive genetic relationship with HUWE1, in contrast to what is expected for a ubiquitin ligase-substrate relationship. We find that HAPSTR1 is required for HUWE1 nuclear localization and targeting of nuclear substrates. Mutations that disrupt HAPSTR1 nuclear localization or HUWE1 binding compromise HUWE1 nuclear activity. Nuclear HUWE1 affects stress signaling pathways, including nuclear factor κB (NF-κB)-mediated inflammatory signaling and p53 signaling. Loss of HAPSTR1 or HUWE1 activates p53 signaling in a manner that depends upon the ability of HAPSTR1 to localize HUWE1 to the nucleus. Further, loss of nuclear HUWE1 activity limits cellular growth, despite total HUWE1 cellular levels remaining unchanged. Together, we demonstrate that critical nuclear HUWE1 ubiquitylation activity is enabled by HAPSTR1.

RESULTS

Proteomic profiling of HUWE1 substrates

HUWE1 has been reported to regulate a diverse and growing number of cellular pathways through the targeted degradation of structurally diverse proteins.[7,8] In order to characterize the mechanisms HUWE1 utilizes to enable such plasticity toward its substrates, we performed quantitative proteomics to identify proteins whose steady-state abundance is elevated upon HUWE1 loss of function. We generated 293T cells with inducible expression of short hairpin RNAs (shRNAs) targeting HUWE1 and validated that the shRNAs substantially reduced HUWE1 protein levels (Figure S1A). We chose the two cell lines with the greatest HUWE1 depletion (155 and 969, hereafter designated shHUWE1–2 and shHUWE1–3, respectively) to perform proteomic profiling of whole-cell extracts using a tandem mass tag (TMT) approach. In total, we quantified more than 8,800 proteins in both HUWE1 knockdown cell lines and determined protein abundance changes compared with

cells expressing an shRNA targeting firefly luciferase (Figures 1A and 1B; Table S1). Only 138 proteins displayed altered abundance (log_2 fold change greater or less than 0.7) in either cell line, and 104 of the 107 proteins that increased in abundance did not have increased mRNA abundance (Table S2). We observed a high correlation between the two HUWE1 shRNA experiments (Figure 1B). Surprisingly, only two previously characterized HUWE1 substrates were identified in this experiment and there was little to no overlap with previous proteomic experiments.[14,31] It is possible that the HUWE1 substrate pool is highly variable across cell lines and conditions or that our HUWE1 depletion, which was around 4-fold, was insufficient to observe significant changes in substrate levels. To directly address the second possibility, we obtained two previously characterized HUWE1 knockout (KO) cell lines.[43] Using quantitative proteomics, we identified 227 proteins that increased in abundance in HUWE1 KO cells compared with HAP1 parental cells (Figure 1C; Table S3). Despite the observation that HUWE1 protein levels were depleted 16-fold (limit of detection), few known HUWE1 substrates were identified. Further, only 21% (23 out of 107) of the proteins that increased in abundance upon HUWE1 shRNA-mediated knockdown also had elevated protein levels in HUWE1 KO HAP1 cells. Taken together, our data suggest that the putative HUWE1 substrate pool varies substantially between cell types and likely varies based on cellular conditions.

C16orf72/HAPSTR1 is a HUWE1 substrate

One protein that accumulated substantially upon both HUWE1 knockdown and KO was C16orf72. This protein was notable due to its known genetic and physical association with HUWE1.[44,45] To validate C16orf72, as well as other identified proteins, as potential HUWE1 substrates, we generated stable FLAG-hemagglutinin (HA)-tagged expression cell lines. The protein levels of stably expressed C16orf72 substantially increased upon proteasome or ubiquitin-activating enzyme (E1) inhibition but not autophagy inhibition (Figure 1D). Validating our proteomic data, HUWE1 siRNA-mediated knockdown elevated C16orf72 protein levels (Figure 1E). Similarly, HUWE1 knockdown elevated the levels of exogenous SCNM1 and MAFB (Figure 1F). Wild-type (WT), but not a catalytically inactive version of HUWE1, ubiquitylates C16orf72 *in vitro*, further substantiating C16orf72 as a HUWE1 substrate (Figures S1B and S1C). A recent study also identified C16orf72 as a HUWE1 substrate and interacting protein that broadly alters the transcription of many stress-responsive proteins, renaming C16orf72 as HAPSTR1, which we adopt here.[46]

HUWE1 cooperates with other ligases to mediate substrate degradation

The breadth of putative HUWE1 substrates, combined with the poor overlap of identified proteins that accumulate upon HUWE1 depletion, suggests that many HUWE1 substrates may be shared with other ubiquitin ligases. To begin to discriminate between putative dedicated versus shared HUWE1 substrates, we employed a knockdown-rescue approach. For this approach, we knocked down endogenous HUWE1 while also transiently expressing exogenous siRNA-resistant HUWE1. Endogenous HUWE1 depletion stabilized both exogenous HAPSTR1 and endogenous DDIT4, a well-characterized HUWE1 substrate (Figure 2A). Expression of exogenous, siRNA-resistant HUWE1 restored HAPSTR1 and DDIT4 degradation (Figure 2A). However, expression of a catalytically inactive version of HUWE1 (C4341S [CS]) failed to rescue HAPSTR1 and DDIT4 degradation (Figure

2A). We further observed that HUWE1 CS overexpression in the presence of endogenous HUWE1 stabilized both HAPSTR1 and DDIT4 (Figure 2A), suggesting that inactive HUWE1 acts in a dominant-negative fashion to inhibit either WT HUWE1 or other cooperating ubiquitin ligases. Interestingly, expression of HUWE1 CS does not appear to act in a dominant-negative manner toward HAPSTR1 when endogenous HUWE1 is depleted (Figure 2A). In contrast, HUWE1 CS expression resulted in stabilization of DDIT4 even in the absence of endogenous HUWE1 (Figure 2A). Taken together, these results suggest that HAPSTR1 is a dedicated HUWE1 substrate, but other HUWE1 substrates, including DDIT4, are shared with other ligases.

Our observation that expression of inactive HUWE1 resulted in putative substrate accumulation led us to globally determine the proteomic changes in cells expressing HUWE1 CS. We used genome engineering to generate a HUWE1 knockin (KI) HAP1 cell line with the CS mutation at the genomic locus. Using our proteomic pipeline, we quantified more than 7,300 proteins. Compared with parental HAP1 cells, 710 proteins displayed altered abundance, with 427 proteins increased in abundance, in the HUWE1 KI cell line. As expected, HAPSTR1 levels were elevated in the HUWE1 KI cells (Figure 2B; Table S3). Of the proteins with elevated protein levels in both HUWE1 KO clones, 66% also had increased protein abundance in HUWE1 KI cells. However, only 17% (19 out of 107) of the proteins that accumulated upon HUWE1 knockdown in 293T cells also displayed elevated protein levels in HAP1 HUWE1 KI cells. Combined, our data suggest that HUWE1 targets a broad and highly cell-type-specific substrate pool, which may be a desired feature for a plastic ubiquitin ligase tasked to broadly regulate disparate pathways and substrates.

HUWE1 structural features differentially enable substrate degradation

We used our knockdown-rescue approach with a collection of HUWE1 mutants to start to understand which HUWE1 sequence and structural features are utilized for substrate targeting. We generated over 20 siRNA-resistant HUWE1 variants containing either mutations in key domains or structural features, or disease-associated mutations, and we tested the ability of each variant to destabilize HAPSTR1 and DDIT4 (Figure S3A; Table S4). HUWE1 contains two separate ubiquitin-binding modules, one consisting of a UIM and a UBA domain, and one built from three repetitive UBM motifs.[13] HAPSTR1 levels were increased by expression of combinatorial mutants eliminating multiple ubiquitin-binding domains, suggesting that the ability of HUWE1 to bind ubiquitin contributes to HAPSTR1 degradation (Figures 2C and S3B). A panel of five HUWE1 mutants observed in patients with intellectual disability disorders largely resembled WT HUWE1 in its ability to target HAPSTR1, with only the Δ168–189 variant compromising HUWE1 function. Two HUWE1 structural mutants (#24 and #32) were also unable to destabilize HAPSTR1, with the deletion of a large unstructured domain impairing HAPSTR1 degradation to the level observed with the catalytically inactive (CS) variant. Interestingly, neither the ubiquitin-binding domains nor the large unstructured domain within HUWE1 were required for HUWE1 to target DDIT4 (Figure 2C). Similarly, a HUWE1 variant lacking all ubiquitin-binding domains retained its ability to target exogenous MAFB (Figures 2D and S3C). These results suggest that diverse structural features within HUWE1 operate in a substrate-specific manner.

A subset of HUWE1 substrates requires HAPSTR1

Examination of DepMap data[45,47,48] revealed a strong positive genetic correlation between HUWE1 and HAPSTR1, as noted by others (Figure 3A).[46] Because ligase-substrate relationships would be predicted to have a negative correlation, the DepMap data suggest that HAPSTR1 is not only a substrate but also a positive regulator of HUWE1 function. To gain insights into how HAPSTR1 regulates HUWE1 function, we measured protein abundance changes upon knockdown of HUWE1 or HAPSTR1 using our unbiased quantitative proteomic pipeline. We utilized CAL27 cells for this approach because CAL27 cells require both HUWE1 and HAPSTR1 for proliferation.[45,47,48] We identified 115 and 106 proteins with increased abundance following HUWE1 or HAPSTR1 knockdown, respectively (Figure 3B; Table S5). Consistent with previous results, putative HUWE1 substrates identified in CAL27 cells were largely unique and not identified in our studies in other cell lines or in previous studies (Figures S2A–S2C). Indeed, across all four HUWE lossof-function proteomics experiments reported here, more than 80% of all putative HUWE1 substrates were identified in only a single experiment (Figure S2B). Furthermore, only one protein displayed increased abundance in all four experiments (Figures S2C). Interestingly, protein abundance changes comparing HUWE1 and HAPSTR1 knockdown in CAL27 cells were significantly correlated, with 40% of putative HUWE1 substrates also accumulating upon HAPSTR1 knockdown (Figure 3B; Table S5). To validate these results, we generated CAL27 cells with stable expression of a subset of identified putative substrates. Despite not identifying HAPSTR1 in our CAL27 proteomic study, we confirmed that HAPSTR1 is a robust HUWE1 substrate in CAL27 cells (Figure 3C). We also validated that SCNM1, MAFB, NFIB, and ZCCHC17 are stabilized upon either HUWE1 or HAPSTR1 knockdown (Figure 3C). We noted variation in the dependence of some putative substrates on HUWE1 versus HAPSTR1. For example, NFIB was stabilized to a greater extent upon HAPSTR1 knockdown compared with HUWE1 knockdown and MAFB was more dependent on HUWE1 than HAPSTR1. Co-depletion of HUWE1 and HAPSTR1 did not result in further protein stabilization for most putative substrates tested, MAFB being the notable exception (Figure 3C). Our data implicate HAPSTR1 as a putative regulator of HUWE1 function and identify HUWE1 substrates that also require HAPSTR1 for degradation.

HAPSTR1 interacts with HUWE1 and nuclear proteins

To examine possible HAPSTR1 regulatory mechanisms, we mapped the physical interactions for HAPSTR1 and HUWE1 using affinity enrichment followed by mass spectrometry. Consistent with previous studies,[44,46,49] HAPSTR1 and HUWE1 interact with each other (Figure 3D). Further, more than 60% of the identified HUWE1-interacting proteins were also identified as HAPSTR1-interacting proteins, with 40% of HAPSTR1 interactors overlapping with HUWE1 interactors (Figures 3E and 3F; Table S6). Interestingly, bioinformatic analyses of HAPSTR1- and HUWE1-interacting proteins revealed an enrichment for nuclear localized proteins and for proteins known to regulate nuclear cytoplasmic transport (Figure 3G). HUWE1-interacting proteins additionally displayed enrichment for proteins involved in proteasomal degradation, including many proteasomal proteins, as previously described.[50] However, these proteasomal proteins were notably absent from the list of HAPSTR1 interactors. This observation, and the finding

that HUWE1 protein levels far exceed HAPSTR1 in nearly all cell and tissue types,[51–53] suggests that HUWE1 likely functions in complexes with and without HAPSTR1.

HAPSTR1 localizes HUWE1 to the nucleus

Combining our interaction data indicating that HAPSTR1 and HUWE1 bind nuclear proteins with our identification of nuclear proteins (SCNM1, MAFB, NFIB, and ZCCHC17) that are stabilized by either HAPSTR1 or HUWE1 loss of function, we speculated that HAPSTR1 may regulate nuclear HUWE1 functions. To test this hypothesis, we first knocked down HUWE1 or HAPSTR1 and biochemically isolated nuclei. Subsequent immunoblotting for endogenous HUWE1 revealed that HAPSTR1 knockdown substantially reduced nuclear HUWE1 levels, resulting in cytoplasmic enrichment (Figures 4A, S4A, and S4B). Consistent with our previous proteomics results, HAPSTR1 knockdown does not change total HUWE1 protein levels (Figure 3B; Table S5). These data suggest that HAPSTR1 plays a role in localizing HUWE1 to the nucleus.

We next sought to define HAPSTR1 mutations that perturb either the HUWE1 interaction or the nuclear localization of HAPSTR1. Sequence comparison of human HAPSTR1 with its putative ortholog in *Saccharomyces cerevisiae* (YJR056C) identified a repeated conserved N-terminal sequence that is contained within two predicted helical domains (Figure 4B). Recent studies mapped a HUWE1 interaction domain (HBO) within this region, and a nuclear localization sequence (NLS) was identified in the C terminus of HAPSTR1.[46] We therefore generated two HAPSTR1 deletion mutants, one without the first 102 amino acids that includes the N-terminal conserved repeated regions (R1 and R2; Δ1–102) and one with the C-terminal NLS deleted (ΔNLS). Stable 293T cell lines expressing WT and the two HAPSTR1 mutants demonstrated elevated HAPSTR1 protein levels for the Δ1–102 variant compared with WT and a further striking increase in protein levels upon NLS deletion (Figures 4C and S4C). Both WT and Δ1–102 HAPSTR1 protein levels increased upon proteasome or ubiquitin-activating enzyme inhibition, as well as upon HUWE1 knockdown (Figures 4C, 4D, and S4C). In contrast, the ΔNLS HAPSTR1 variant was not stabilized by proteasome inhibition or HUWE1 knockdown (Figures 4C, 4D, and S4C). Consistent with these observations, ΔNLS HAPSTR1 was not robustly polyubiquitylated by HUWE1 *in vitro* (Figure S4D). While similar results were observed in CAL27 cells with stable expression of WT or mutant HAPSTR1, Δ1–102 HAPSTR1 was expressed at levels lower than observed in 293T cells (Figures S4E–S4G). WT HAPSTR1 interacted with HUWE1 in co-immunoprecipitation (coIP) experiments and this interaction was substantially compromised, but not eliminated, upon deletion of either the N-terminal 102 amino acids or the C-terminal NLS (Figure 4E). This result suggests that, while the N terminus contributes to HUWE1 binding, sequences beyond the repeated regions, such as the larger HBO domain, as well as the C-terminal NLS, contribute critical HUWE1-binding surfaces.

To further test if HAPSTR1 localizes HUWE1 to the nucleus, we examined exogenous HUWE1 cellular localization by microscopy with and without HAPSTR1 co-expression. HUWE1 was largely localized to the cytoplasm while HAPSTR1 was nuclear when expressed in isolation (Figures 4F and 4G). Upon co-expression, WT HAPSTR1 strikingly

relocalized co-expressed HUWE1 to the nucleus (Figures 4F and 4G). HUWE1 co-expression with the Δ1–102 variant of HAPSTR1 did not result in HUWE1 nuclear localization, despite Δ1–102 HAPSTR1 maintaining its nuclear localization. As expected, ΔNLS HAPSTR1 was relocalized to the cytoplasm and failed to enrich HUWE1 within the nucleus (Figures 4F and 4G). In total, our results demonstrate that HAPSTR1 is required for nuclear localization of HUWE1.

HAPSTR1 potentiates nuclear HUWE1 activity

Because nuclear HUWE1 levels are regulated by HAPSTR1, we examined whether the ability of HUWE1 to target nuclear substrates was similarly regulated by HAPSTR1. We used a knockdown-rescue approach in cell lines with stable expression of siRNA-resistant, FLAG-HA-tagged WT, Δ1–102, or ΔNLS HAPSTR1. We then expressed two substrates, MAFB and SCNM1, in these HAPSTR1-expressing cell lines with or without knockdown of endogenous HAPSTR1. Endogenous HAPSTR1 knockdown elevated MAFB and SCNM1 protein levels, and reexpression of WT HAPSTR1 largely eliminated the increase in MAFB or SCNM1 levels upon endogenous HAPSTR1 knockdown (Figures 5A and 5B). The Δ1–102 and the ΔNLS HAPSTR1 variants did not rescue MAFB nor SCNM1 degradation, with the ΔNLS version acting in a dominant-negative fashion with regard to MAFB degradation (Figures 5A and 5B). Based on our observation that there may be some HUWE1-independent roles for HAPSTR1, at least with regard to MAFB degradation (Figure 3C), we examined MAFB stabilization with HUWE1/HAPSTR1 co-depletion in our HAPSTR1 rescue system. Reintroduction of WT HAPSTR1, but not Δ1–102 or ΔNLS, restores MAFB levels to the levels observed with HUWE1 depletion alone (Figure 5C). These data suggest that HAPSTR1 largely operates within a HUWE1 context but that both factors may operate independently from each other in some contexts.

To test if nuclear localization was a critical determinant for HAPSTR1-dependent HUWE1 degradation, we deleted a predicted importin α-dependent nuclear localization signal from SCNM1 (Δ1–24). Compared with WT SCNM1 localization, SCNM1 Δ1–24 displayed enhanced cytoplasmic localization (Figure 5D). Knockdown of HUWE1 or HAPSTR1 stabilized WT SCNM1, but HAPSTR1 knockdown failed to stabilize SCNM1 Δ1–24 (Figures 3C and 5D). Consistent with previous observations that HAPSTR1 depletion did not result in protein accumulation of known cytoplasmic HUWE1 substrates,[46] these results suggest that loss of HAPSTR1 restricts HUWE1 localization to the cytoplasm, thereby affecting HUWE1's ability to target nuclear, but not cytoplasmic, substrates.

We next asked if nuclear HUWE1 activity is required to support overall cell proliferation. We generated CAL27 cells with doxycycline-inducible Cas9 expression and stable expression of an sgRNA targeting HUWE1 or HAPSTR1. We confirmed that Cas9 expression in cells expressing a HUWE1-targeting sgRNA resulted in decreased HUWE1 protein levels (Figures S5A and S5B). To determine the effect of HUWE1 or HAPSTR1 KO on cellular proliferation, we used a competitive growth assay in which control GFP-expressing CAL27 cells were mixed 1:1 with iCas9-expressing cells (Figure 5E). Expression of an sgRNA targeting HUWE1 or HAPSTR1, but not the control sgRNA, resulted in a doxycycline-dependent decrease in cell proliferation (Figure 5E). Re-expression of sgRNA-

resistant WT, but not the Δ1–102 or ΔNLS HAPSTR1 variants, rescued the repression of cell proliferation upon targeting of the endogenous HAPSTR1 locus (Figures 5E and S5A). These results argue that loss of nuclear HUWE1 represses cell proliferation in CAL27 cells. To examine possible HUWE1-independent roles for HAPSTR1, we tested the impact of co-depletion of HUWE1 and HAPSTR1 on cell proliferation. We constructed a dual gRNA-expressing plasmid that expressed both HUWE1- and HAPSTR1-targeting gRNA. The proliferation of cells co-depleted of HUWE1 and HAPSTR1 was slightly worse than in single-depletion experiments, suggesting there is likely some minor HUWE1- independent effect upon HAPSTR1 depletion (Figure S5C). However, this result also suggests that the observed proliferation defect in the depletion of HUWE1 or HAPSTR1 is largely attributed to the overlapping function of HUWE1 and HAPSTR1.

Nuclear HUWE1 broadly regulates a stress-dependent transcriptional program

To more broadly examine the role of nuclear HUWE1, we performed RNA sequencing (RNA-seq) in CAL27 cells after siRNA-mediated knockdown of HUWE1 or HAPSTR1. Loss of either HUWE1 or HAPSTR1 resulted in broad transcriptional changes, with 845 and 677 significantly differentially expressed genes observed upon HUWE1 or HAPSTR1 knockdown, respectively (Figures 6A–6C and S6A; Table S7). We noted a correlation between the altered transcripts upon HUWE1 or HAPSTR1 knockdown, with 405 shared differentially expressed genes, suggesting that loss of HAPSTR1 or HUWE1 affects similar transcriptional pathways (Figures 6A–6C, S6A, and S6B). The majority of observed protein level changes in our CAL27 proteomics dataset were not observed on the transcript level, although some protein level changes were likely the combined result of altered protein turnover and increased mRNA abundance (Figures S6C and S6D). Pathway enrichment analysis of differentially expressed genes revealed repression of many genes involved in innate immunity and inflammatory signaling upon loss of HUWE1 or HAPSTR1 (Figures 6D and 6E). These results are broadly consistent with a recent study demonstrating that similar stress-responsive transcriptional pathways are affected by either loss of HUWE1 or HAPSTR1.[46]

The noted enrichment of inflammatory genes that were repressed upon HUWE1 or HAPSTR1 knockdown suggested that nuclear HUWE1 may potentiate activation of innate immune signaling pathways (Figures 6E and 6F). Mining the list of altered transcripts for enrichment of transcription factor binding sites revealed NF-κB target genes to be strongly represented within the differentially expressed genes (Figure 6G).[54] Examination of all known NF-κB targets revealed a significant repression among a broad range of NF-κB targets upon HUWE1 knockdown, and to a lesser extent HAPSTR1 knockdown (Figures 6G and 6H). We then turned to an NF-κB reporter system to directly test whether HUWE1 or HAPSTR1 knockdown repressed baseline or TNFα-stimulated NF-κB signaling.[55] Knockdown of either HUWE1 or HAPSTR1 repressed baseline NF-κB transcriptional activity with HUWE1 but not HAPSTR1 affecting the TNFα-stimulated response (Figure 6I). These results are consistent with previous studies demonstrating that loss of HUWE1 suppresses NF-κB activity.[56] We then used qPCR and confirmed that the mRNA levels of two NF-κB targets, CCL20 and CXCL3, were repressed in unstimulated CAL27 cells upon knockdown of either HUWE1 or HAPSTR1 (Figure 6J). Further, we demonstrated

that the observed repression of CCL20 and CXCL3 expression upon HAPSTR1 knockdown was reversed upon reexpression of WT, but not Δ1–102 or ΔNLS, HAPSTR1 variants (Figure 6J). These results indicate that loss of nuclear HUWE1 activity is likely responsible for the observed transcriptional repression of inflammatory signaling components. Taken together, our results demonstrate that nuclear HUWE1 potentiates NF-κB activity under basal conditions and may widely regulate inflammatory signaling and responses.

Loss of nuclear HUWE1 activates p53 signaling and limits cell proliferation

A closer examination of the DepMap data revealed that cell lines with WT p53 broadly showed an increased dependence on HUWE1 or HAPSTR1 for proliferation compared with cells containing “hotspot” p53 mutations known to inactivate p53 transcriptional activity (Figure 7A). Further, DepMap correlations between HUWE1, HAPSTR1, and known p53 positive and negative regulators revealed a similarity between MDM2, a known negative regulator of p53 signaling, and HAPSTR1 (Figures 7A and 7B). These observations, along with previous studies, suggest that HAPSTR1 may negatively regulate p53 signaling.[10,32,34,37,49] To directly test whether HUWE1 or HAPSTR1 negatively regulate p53 signaling, we knocked down HUWE1 or HAPSTR1 in p53 functional HCT116 or RPE1 cells. Consistent with previous studies, both HUWE1 and HAPSTR1 knockdown increased p53 levels (Figures 7C and S7A).[10,49] Despite a clear induction of DNA damage response pathways upon etoposide or cisplatin treatment in p53 WT or null HCT116 cells (Figure S7B), loss of HUWE1 or HAPSTR1 did not result in a basal increase in γH2AX phosphorylation. These results suggest that loss of HUWE1 or HAPSTR1 may directly affect p53 signaling independent of the DNA damage response.

To examine if nuclear HUWE1 was responsible for repressing p53 activity, we generated HCT116 (WT p53) cells with stable expression of siRNA-resistant WT, Δ1–102, or ΔNLS HAPSTR1. Δ1–102 HAPSTR1 expression levels were lower than WT HAPSTR1, precluding further functional analysis (Figure 7D). Re-expression of WT, but not ΔNLS, HAPSTR1 rescued the increase in p53 levels upon endogenous HAPSTR1 knockdown (Figure 7D). This result is consistent with the hypothesis that nuclear HUWE1 represses p53 levels. Indeed, loss of HUWE1 resulted in a further repression of cell proliferation upon cisplatin treatment in a p53-dependent manner (Figure S7C). Overall, our results demonstrate that HAPSTR1 acts to localize HUWE1 to the nucleus to regulate a likely broad swath of nuclear targets affecting inflammatory and p53 signaling pathways.

DISCUSSION

HUWE1 substrate plasticity and pleiotropic functions

HUWE1 is an enigmatic ubiquitin ligase that has been implicated in numerous cellular pathways, including DNA repair, transcription, proliferation, apoptosis, and cell signaling.[7] Further, HUWE1 has been described to both promote and restrict tumorigenesis, as well as to play critical roles in neurodevelopmental pathways.8,9,24,25,29,30,32,33,35–38,57,58 These pleiotropic functions for HUWE1 suggest that it targets a diverse, and likely context-specific, set of substrates for ubiquitylation. Our unbiased proteomic approach demonstrating a surprising lack of common HUWE1 substrates supports the hypothesis that

HUWE1 targets diverse substrates for degradation in a cell-type-specific manner. It is also likely that other ligases act on a similarly broad set of substrates, which may compensate for loss of HUWE1 in our and other studies. Indeed, our demonstration that overexpression of catalytically inactive HUWE1 results in a greater accumulation of substrates compared with HUWE1 loss of function supports the idea that HUWE1 acts in concert with other ligases.

HUWE1 substrate-targeting mechanisms

How broadly acting ubiquitin ligases target their substrates is an open question. Despite amazing progress in our understanding of protein ubiquitylation and degradation mechanisms, the substrate-targeting mechanisms of only a small fraction of the over 600 ubiquitin ligases encoded within the human genome have been studied in detail. The diverse domain organization within HUWE1 includes three different ubiquitin-binding domains, a WWE domain, and a BH3 domain. It is suggested that HUWE1 recruits diverse substrates using these domains. The demonstration that the HUWE1 armadillo repeats can engage the flexible N terminus of DDIT4 indicates that HUWE1 can also bind substrates within the central cavity of the structural ring.[13] These observations establish a possible mechanism in which HUWE1 engages a structurally highly diverse set of substrates and positions them within the central cavity to allow the HECT domain to catalyze ubiquitylation.

The budding yeast HUWE1 ortholog, Tom1, also contains a ubiquitin-binding domain and armadillo repeats, suggesting that the overall structure and substrate-targeting mechanisms may be conserved. The expansion of the ubiquitin-binding domains within human HUWE1 suggests that HUWE1 may engage substrates that were previously ubiquitylated by other ubiquitin ligases. Tom1 was recently shown to act in an E4-like mechanism to target a model ubiquitin-fusion degradation (UFD) substrate for degradation.[59] In addition, HUWE1 and TRIP12, another pleiotropic HECT-domain ligase, were demonstrated to target a UFD reporter substrate in human cells, arguing that HUWE1 may amplify ubiquitin chains on substrates previously ubiquitylated by other ligases.[60] Binding preexisting ubiquitin chains may also allow HUWE1 to build branched ubiquitin chains on substrates to accelerate proteasome targeting, a property that has been described for HUWE1, TRIP12, and the HUWE1 ortholog Tom1.[56,59,61–63] This possible E4 mechanism for HUWE1 is also consistent with the notion that HUWE1 may not have many dedicated substrates.

HAPSTR1 regulates HUWE1 nuclear activity

The positive genetic relationship between HUWE1 and HAPSTR1 suggested that HAPSTR1 regulates HUWE1 function. Our findings that HAPSTR1 acts to localize HUWE1 to the nucleus, and that nuclear HUWE1 is required for cell proliferation, explains the genetic relationship. Our finding that HAPSTR1 is both a HUWE1 substrate and a HUWE1 regulator suggests a negative feedback mechanism in which HAPSTR1 recruits HUWE1 to the nucleus to target diverse nuclear substrates, including HAPSTR1 itself.

Loss of HUWE1 or HAPSTR1 affects diverse transcriptional pathways, including NF-κB-mediated inflammatory signaling. The mechanism by which HUWE1 activates baseline inflammatory signaling remains largely uncharacterized. While loss of HUWE1 and HAPSTR1 represses the transcription of many chemokines and cytokines, HAPSTR1

depletion was also shown to reduce overall chemokine secretion and cell migration.[46] Our analysis also revealed enrichment for cell motility factors in transcripts repressed by loss of HAPSTR1, which suggests that cell migration may be broadly affected by transcriptional programs regulated by nuclear HUWE1 activity.

Limitations of the study

The HUWE1 antibody used here for immunoblotting displays non-specific immunofluorescence staining. Thus, our ability to rigorously assess endogenous HUWE1 localization has been limited by the currently available HUWE1 antibodies. Additionally, other than for HAPSTR1, we have not shown that the identified proteins whose abundance increased upon HUWE1 loss of function are directly ubiquitylated by HUWE1. Finally, we have not identified the mechanism by which the broad stress signaling response is modulated by nuclear HUWE1 activity. Thus, future studies will be required to investigate the mechanisms of HUWE1 substrate selection and nuclear targeting.

STAR★METHODS

RESOURCE AVAILABILITY

Lead contact—Further information and requests for resources and reagents should be directed to and will be fulfilled by the lead contact, Eric Bennett (e1bennett@ucsd.edu).

Materials availability—All reagents generated in the study are available from the lead contact with a completed Materials Transfer Agreement.

Data and code availability—Proteomics data have been deposited at PRIDE and RNA-seq data have been deposited at Zenodo and are publicly available as of the date of publication. Accession numbers/DOIs are listed in the key resources table.

This paper does not report original code.

Any additional information required to reanalyze the data reported in this paper is available from the lead contact upon request.

EXPERIMENTAL MODEL AND STUDY PARTICIPANT DETAILS

293T (female), CAL27 (male), and HCT116 (male) cells were grown in DMEM (high glucose, pyruvate and L-glutamine) supplemented with 10% fetal bovine serum, 100 U/mL penicillin and 100 U/mL streptomycin. HAP1 (male-derived, lacking a Y chromosome) cells were grown in IMDM supplemented with 10% fetal bovine serum, 100 U/mL penicillin and 100 U/mL streptomycin. HAP1 HUWE1 KO clone3 and clone5, and parental cells were gifts from David Toczyski (UCSF). NCI-H2052 (male) cells were grown in RPMI supplemented with 10% fetal bovine serum, 2 mM glutamine, 100 U/mL penicillin and 100 U/mL streptomycin. RPE1 (female) cells were grown in DMEM:F-12 supplemented with 10% fetal bovine serum, 100 U/mL penicillin and 100 U/mL streptomycin. All cells were cultured at 37°C with 5% CO_2 and tested for mycoplasma contamination monthly.

METHOD DETAILS

Reagents—Chemical reagents were used at the following concentrations: Doxycycline, 5 μg/mL; Bafilomycin A1, 100 nM; MG132, 10 μM. TAK-243, 1 μM. Etoposide, 50 μM. Cisplatin, 12.5 μM.

Plasmids—Plasmids containing doxycycline-inducible shRNAs were obtained from Dharmacon. pDONR plasmids containing HAPSTR1, SCNM1, NFIB, MAFB and ZCCHC17 were obtained from the human ORFeome collection.[66] Stop codons were introduced by site-directed mutagenesis, verified by sequencing, and then cloned into expression vectors by Gateway cloning. HUWE1 variants were generated by Gibson assembly (New England Biolab).[13] To generate siRNA resistant HAPSTR1 cDNA, silent mutations were introduced within the region recognized by HAPSTR1 siRNA oligo #1 by site-directed mutagenesis. HAPSTR1 ΔNLS contains amino acids 1–251 and was generated by PCR amplification and recombination into a Gateway expression plasmid. For transient transfections, constructs were cloned into pDEST_CMV_FLAG. For stable expression, constructs were cloned into pDEST_pHAGE_FLAG-HA_IRES_PURO, pDEST_pHAGE_FLAG-HA_IRES_mCherry, or pDEST_pHAGE_GFP_PGK_BLAST. For purification, constructs were subcloned using Gibson assembly into modified pDARMO (pDarmo.CMVT_v1 was a gift from David Sabatini [Addgene plasmid #133072]) plasmids with N-terminal FLAG- and Strep-tags for expression in Expi293 (Thermo Fisher Scientific, A14635), or into pAC8-derived vectors[67] for expression in insect cells.

Cell lines, transfections, and siRNA—Lentiviruses were produced by transfection of 293T cells with Mirus TransIT 293 transfection reagent. Cell lines with stable transgene expression were generated by lentiviral infection followed by puromycin (inducible shRNA and pHAGE_FLAG-HA plasmids) or blasticidin selection (pHAGE_GFP plasmids).

Lipofectamine 2000 (Thermo Fisher) was used according to the manufacturer's protocol for transient transfections of plasmids or co-transfection of plasmid and siRNA. Cells were collected 2 days after plasmid transfection or 3 days after plasmid and siRNA co-transfection. Lipofectamine RNAiMAX (Thermo Fisher) was used according to the manufacturer's protocol for siRNA transfections, with cells collected 3 days after transfection. Inducible shRNA samples were collected 4 days after addition of doxycycline.

Protein purification—Recombinant FLAG-HUWE1 was prepared as described previously.[13] Briefly, Expi293 cells were harvested, lysed in lysis buffer (50 mM HEPES/KOH, pH 7.4, 200 mM NaCl, 5% glycerol, protease inhibitors), cleared by ultracentrifugation, and incubated with FLAG-antibody-coated beads. Beads were washed and bound protein was eluted with FLAG peptide. The protein was concentrated and polished by size exclusion chromatography. Strep-HUWE1, FLAG-SCNM1 and Strep-HAPSTR1 (aa 1–251) were transiently expressed in Expi293 following the manufacturer's manual. Full-length Strep-HAPSTR1 was expressed in *Trichoplusia Ni* High Five insect cells (Thermo Fisher Scientific) infected with baculovirus produced in *Spodoptera frugiperda* Sf9 cells. Cells were harvested 48–60 h post transfection/infection and lysed by sonication in lysis buffer. After clearance by ultracentrifugation (45 min, 120,000 g)

the lysates were incubated with either FLAG-antibody-coated beads (Genscript, L00432) or Strep-TactinXT 4Flow high-capacity resin (IBA life sciences, 2–5030-002). Bound proteins were eluted with 0.2 mg/mL 1xFLAG peptide (DYKDDDDK) or 50 mM biotin, respectively. Proteins were concentrated using centrifugal concentrators (Amicon, 10 kDa molecular weight cut-off (MWCO)). Full-length Strep-HAPSTR1 and Strep-HUWE1 were additionally purified by anion exchange chromatography (PorosHQ, Thermo Fisher Scientific, 1255911) prior to final polishing. All proteins were polished by size exclusion chromatography on either Superdex75Increase 10/300 (GE Healthcare) or Superose6 Increase 10/300 (GE Healthcare) in 30 mM HEPES/KOH, pH7.4, 150 mM NaCl, 3 mM Tris(2-carboxyethyl)phosphine).

***In vitro* ubiquitylation assay—**0.5 μM UBE2D2 (R&D Systems) was charged with ubiquitin for 30 min by the addition of 1X E3 Ligase Conjugation Buffer (R&D Systems), 0.2 μM UBE1 (R&D Systems), 50 μM ubiquitin (R&D Systems), and 10 mM MgATP (R&D systems). *In vitro* ubiquitylation reactions were initiated by addition of 2 μM Strep-HAPSTR1 variant or FLAG-SCNM1 and 0.2 μM FLAG-HUWE1 or Strep-HUWE1, respectively. Reactions were allowed to proceed at the indicated temperature for 20 min, quenched by addition of reducing SDS dye and analyzed via immunoblot with a 1:16,000 dilution of an anti-Strep HRP conjugate (Fisher Scientific) or with a 1:1000 dilution of an anti-FLAG M2 antibody (Sigma Aldrich, F3165). Blots were imaged on an Amersham Imager 600 using Amersham ECL Prime Western Blotting Detection Reagent (GE Life Sciences) or on an LI-COR Odyssey CLx detecting an anti-mouse secondary antibody (LI-COR, 926–68070).

HAP1 HUWE1 C4341S knock-in clone generation—Hap1 HUWE1-C4341S-KI was generated via prime editing at the endogenous site. The pegRNA sequence was designed with an online tool (http://deepcrispr.info/DeepPE/) and the following sequences were selected: protospacer sequence: 5′-GCCTGCCTTCAGCTCACACA-3′; reverse transcription template including edit: 5′-CTTTTACgATGT-3′; primer-binding site: 5′-GTGAGCTGAAGGC-3′. The plasmid expressing pegRNA was cloned via Gibson assembly using a gBlock gene fragment containing the U6 promoter and the pegRNA sequence (purchased from IDT) and a linearized pBluescript vector. Hap1 cells were seeded in 6-well plates and transfected at roughly 70% confluency with lipofectamine 3000 (Invitrogen) according to the manufacturer's instructions and 500 ng pegRNA plasmid and 1 μg PE plasmid expressing the prime editor (PE2–2A-GFP, Addgene #132776). Cells were cultured for 3 days following transfection and GFP+ single cells were isolated into individual wells of 96-well plates by fluorescence-activated cell sorting (FACS). Cells were expanded for 10 days before genotyping. Genomic DNA was extracted and the editing site was amplified with PCR using the forward primer 5′-GTCCCTTCCTACAGATCCAGTG-3′ and the reverse primer 5′CATCAAGTATGCAAGCTCAACC-3′. The PCR products were first screened using digestion by NlaIII and the potential hits were verified by Sanger sequencing.

Cal27-Cas9 clone, Cal27 iCas9 sgRNA and transgene-expressing cell line generation—Cal27 clones expressing doxycycline-inducible 3xFLAG-Cas9 were

generated by lentiviral infection with pCW-Cas9-Blast (Addgene, #83481), selection with 5 μg/mL Blasticidin for seven days, and dilution to yield individual clones. Clones were analyzed for doxycycline-inducible Cas9 expression by Western blot over several weeks. The iCas9 sgRNA pools were generated by lentiviral infection of the Cal27-Cas9 clone with LentiGuide-Puro expressing the specific gene-targeting Grna. The guide sequences were as follows: control guide 5′-GCATCGTACGCGTACGTGTT-3′, HUWE1 guide 5′-TCCAGTGCGAGTTATATCAC-3′, HAPSTR1 guide 5′-CGGGAGGCCGCGGAGGATGG-3′. Plasmids expressing sgRNAs were constructed by ligation of the annealed oligonucleotides into linearized LentiGuide-Puro vector (Addgene, #52963). Integration of the sgRNA was selected with 1 μg/mL puromycin for seven days and the iCas9 sgRNA pool was analyzed for doxycycline-inducible Cas9 expression by Western blot. The pool targeting HUWE1 was also analyzed for reduced Huwe1 expression by Western blot. The transgene-expressing cell lines were generated with lentiviral infection of the iCas9 sgHAPSTR1 pool with plasmids expressing the Flag-tagged transgene and mCherry fluorescence protein. The mCherry+ pools were isolated by FACS.

GFP-based and internally controlled competitive growth assay—Constitutively GFP-expressing Cal27 cells were generated by lentiviral infection with GFP-IRES-Blast, selection with 5 μg/mL Blasticidin for seven days, and dilution to yield individual cells that highly expressed GFP. The clonal population was checked for sustained GFP expression by flow cytometry. The iCas9 sgRNA pools and GFP+ clone were first treated with 3 μg/mL doxycycline for 3 days individually. Then, the iCas9 sgRNA pools were mixed with the GFP+ clone at approximately equal GFP+ to GFP− ratios and the GFP−/GFP+ ratios were analyzed by flow cytometry on day zero when cells were mixed and day three. Data were analyzed using FlowJo and the GFP−/GFP+ ratios were normalized to the day zero ratio first. The ratios for sgRNA pools were further normalized to that of sgControl.

Immunoblotting—Cell pellets were resuspended 8 M urea, 50 mM Tris pH 8.0, 75 mM NaCl, 1 mM β-glycerophosphate, 1 mM NaF, 1 mM NaV, 40 mM NEM and EDTA-free protease inhibitor cocktail (Roche Diagnostics), sonicated, and cleared by centrifugation at 15,000 rpm for 10 min at 4°C. Protein concentrations were determined by BCA Protein assay (Thermo Fisher). Samples were separated by SDS-PAGE and transferred to PVDF membranes (Bio-Rad) with a semi-dry transfer apparatus (Bio-Rad Turbo Transfer). Membranes were blocked with 4% milk in TBST. Primary antibodies were diluted in 5% BSA in TBST. HRP-conjugated secondary antibodies were diluted in 4% milk in TBST. Immunoblots were developed with Clarity Western ECL Substrate (Bio-Rad) and imaged on a Bio-Rad Chemi-Doc XRS+ system.

Nuclei isolation—Nuclei were isolated as described prevously.[68] Briefly, the following buffers were used: Low-salt wash buffer (10 mM HEPES-KOH pH 7.9, 10mM KCl, 1.5 mM $MgCl_2$, 0.1 mM EDTA, 1 mM β-glycerophosphate, 1 mM NaF, 1 mM NaV, 40 mM NEM and EDTA-free protease inhibitor cocktail (Roche Diagnostics)), Hypo-osmotic lysis buffer (Low-salt wash buffer +0.3 M sucrose, 2% (v/v) Tween 40), 1.5 M sucrose buffer (Low-salt wash buffer +1.5 M sucrose), and High-salt extraction buffer (20 mM HEPES-KOH pH

7.9, 40 mM NaCl, 1.5 mM $MgCl_2$, 0.2 mM EDTA, 25% glycerol). Buffers and samples were kept on ice throughout the protocol. Cell pellets were resuspended in hypo-osmotic lysis buffer and homogenized by pipetting 100 times using a micropipette with a 200-μL pipette tip. The samples were overlaid on 1 mL of 1.5 M sucrose buffer and centrifuged at 12,000 rpm for 10 min at 4°C. After centrifugation, a volume equal to the amount of lysis buffer used was pipetted off the top of sample and saved as the cytoplasmic fraction. The rest of the supernatant was discarded and the nuclear pellets were resuspended in 1 mL of low-salt wash buffer. The nuclei were pelleted by centrifugation at 12,000 rpm for 30 s at 4°C. The supernatant was removed and the washed nuclear pellets were resuspended in high-salt extraction buffer and incubated on ice for 20 min with occasional vortexing. The nuclei were centrifuged at 12,000 rpm for 20 min at 4°C. The supernatants were retained as high-purity nuclear proteins. Nuclear proteins were spotted onto PVDF using a dot blot apparatus. Cytoplasmic proteins were separated by SDS-PAGE.

Immunofluorescence—Cells were grown on glass coverslips coated with poly-L-lysine (Corning Cat# 354085) and fixed with 4% formaldehyde in phosphate-buffered saline (PBS) for 10 min. Blocking and primary antibody dilutions were done in AbDil (20 mM Tris, 150 mM NaCl, 0.1% Triton X-100, 3% bovine serum albumin, and 0.1% NaN_3, pH 7.5). PBS with 0.1% Triton X-100 (PBS-TX) was used for washes and secondary antibody dilutions. Hoechst-33342 was used to visualize DNA. Coverslips were mounted in Fluoromount-G and sealed with nail polish.

Fluorescence microscopy—Images were acquired on an SP8 confocal microscope (Leica Microsystems) with a 63× objective. Images were maximally projected from five z sections with 1 μm spacing using Fiji.[69] The fluorescence is scaled independently in each panel to better show the localization of each transgene.

DNA colocalization measurements were determined with CellProfiler image analysis software.[70]

Immunoprecipitations—For IP-MS experiments, FLAG-tagged HUWE1 or HAPSTR1 expressing cells were resuspended in 50 mM Tris pH 8.0, 200 mM NaCl, 2 mM TCEP, 0.1% NP-40, cOmplete Protease Inhibitor Cocktail (Roche Diagnostics). Cells were lysed by passing through a needle at least 20 times. Samples were centrifuged at 15,000 rpm for 10 min at 4°C. Protein concentrations were determined by BCA Protein assay (Thermo Fisher). Equal concentrations of each sample were incubated with M2-FLAG magnetic beads for 1 h at 4°C. The beads were washed three times with 50 mM Tris pH 8.0, 2 mM TCEP, 0.1% NP-40, cOmplete Protease Inhibitor Cocktail (Roche Diagnostics). Protein was eluted by two incubations with occasional mixing in 0.1 M glycine HCl pH 2.7 for 20 min at room temperature. Elutions were treated with 35 mM TCEP for 30 min, followed by 150 mM iodoacetamide for 45 min, and then 200 mM DTT for 15 min. Proteins were precipitated with methanol/chloroform. Precipitated protein was resuspended in 200 mM EPPS pH 8.0. Proteins were digested with LysC and trypsin overnight at 37°C. Formic acid was added to each sample to a final concentration of 0.7%. Samples were desalted using a SoLa plate (Thermo Scientific) and analyzed by LFQ mass spectrometry.

For IP samples that were analyzed by Western blotting, cells were lysed by incubating on ice in 50 mM Tris pH 8.0, 150 mM NaCl, 0.5% NP-40, 1 mM β-glycerophosphate, 1 mM NaF, 1 mM sodium orthovanadate, 40 mM NEM and cOmplete EDTA-free protease inhibitor cocktail (Roche Diagnostics). Lysates were cleared by centrifugation at 15,000 rpm for 10 min at 4°C. Protein concentrations were determined by BCA Protein assay (Thermo Fisher). Equal concentrations of each sample were incubated with anti-HA agarose beads for 1 h at 4°C. The beads were washed four times with 50 mM Tris pH 8.0, 150 mM NaCl, 0.1% NP-40. To elute, beads were boiled in Laemmli sample buffer.

Luciferase reporter assay—293T cells were reverse transfected with siRNA using Lipofectamine RNAiMAX (Invitrogen) according to the manufacturer's instructions and seeded in 24-well plates. 48 h after siRNA transfection, cells were transfected with the reporter plasmid hRluc-NF-κB-firefly (Addgene, #106979) using Lipofectamine 2000 according to the manufacturer's instructions. Some cells were treated with TNF-α(100 ng/mL) for 6 h before being harvested. 24 h after plasmid transfection, luciferase activity was measured with the Dual-Glo Luciferase Assay System (Promega) according to the manufacturer's instructions. Firefly luciferase activity was normalized to that of Renilla luciferase.

CellTiter-Glo assay—HCT116 cells were reverse transfected with siRNA using Lipofectamine RNAiMAX (Invitrogen). 24 h after transfection, cells were treated with 12.5 μM cisplatin. Cell proliferation was measured 72 h after drug treatment using the CellTiter-Glo 2.0 assay according to the manufacturer's instructions.

qRT-PCR analysis—Total RNA was extracted from Cal27 cells with TRIzol reagent (Invitrogen). 1.5 mg of total RNA was reverse transcribed with the oligo$(dT)_{20}$ and Super-Script III First-Strand Synthesis System (Life Technologies). qRT-PCR was performed using an iTaq SYBR Green mix (Bio-Rad) and the CFX96 Real-Time PCR Detection System (Bio-Rad). The samples were run in biological triplicates and normalized to the internal control GAPDH. The primers were as follows: *CCL20* forward, 5′-AACCATGTGCTGTACCAAGAG-3′; *CCL20* reverse, 5′-CAGTCAAAGTTGCTTGCTTCTG-3′; *CXCL3* forward, 5′-GCAGGGAATTCACCTCAAGA-3′; *CXCL3* reverse, 5′-GTGTG GCTATGACTTCGGTT-3′; *GAPDH* forward, 5′-GGTGGTCTCCTCTGACTTCAACA-3′; *GAPDH* reverse, 5′-GTTGCTGTAGCCAA ATTCGTTGT-3′.

TMT mass spectrometry—293T and HAP1 samples were processed for TMT mass spectrometry. Cell pellets were resuspended in 8 M Urea, 50 EPPS pH 8.5, 50 mM NaCl, 1 mM β-glycerophosphate, 1 mM NaF, 1 mM sodium orthovanadate, and EDTA-free protease inhibitor cocktail (Roche Diagnostics). Cells were lysed with 10 passes through a 21G and cleared by centrifugation at 15,000 rpm for 10 min at 4°C. Protein concentrations were determined by BCA Protein assay (Thermo Fisher). Lysates were treated with 10 mM TCEP for 30 min, followed by 15 mM iodoacetamide for 45 min, and finally 10 mM DTT for 15 min 200 μg of protein for each sample was precipitated using methanol/chloroform as previously described.[71] Precipitated protein was resuspended in 8 M Urea, 50 mM HEPES

pH 7.4, followed by dilution to 1.85 M urea with the addition of 200 mM EPPS, pH 8. Proteins were digested with LysC overnight at room temperature. The next day, the digestions were diluted two-fold with 200 mM EPPS pH 8 followed by digestion with trypsin for 6 h at 37°C. Anhydrous acetonitrile (ACN) was added to each sample to a final concentration of 10% v/v. Tandem mass tag (TMT) reagents (Thermo Fisher Scientific) were dissolved in ACN and added to each sample for 90 min at room temperature. The reaction was quenched with hydroxylamine for 15 min at room temperature. Each channel was combined in a 1:1 ratio, desalted using the Stage-Tip method and analyzed by LC-MS for channel ratio comparison. Samples were then combined using the adjusted volumes determined in the channel ratio analysis and dried down in a speed vacuum. The combined sample was then resuspended in 1% formic before desalting with C18 (Sep-Pak, Waters).

Data were collected using an Orbitrap Fusion Lumos mass spectrometer (Thermo Fisher Scientific, San Jose, CA, USA) coupled with a Proxeon EASY-nLC 1200 LC lump (Thermo Fisher Scientific, San Jose, CA, USA). Peptides were separated on a 50 cm 75 μm inner diameter EasySpray ES803a microcapillary column (Thermo Fisher Scientific). Peptides were separated over a 190 min gradient of 6–27% acetonitrile in 1.0% formic acid with a flow rate of 300 nL/min.

Quantification was performed using an MS3-based TMT method as described previously.[72] The data were acquired using a mass range of m/z 340–1350, resolution 120,000, AGC target 5 × 105, maximum injection time 100 ms, dynamic exclusion of 120 s for the peptide measurements in the Orbitrap. Data dependent MS2 spectra were acquired in the ion trap with a normalized collision energy (NCE) set at 35%, AGC target set to 1.8 × 104 and a maximum injection time of 120 ms. MS3 scans were acquired in the Orbitrap with HCD collision energy set to 55%, AGC target set to 2 × 105, maximum injection time of 150 ms, resolution at 50,000 and with a maximum synchronous precursor selection (SPS) precursors set to 10.

TMT quantitative LC/MS data analysis and statistical analysis—Proteome Discoverer 2.2 (Thermo Fisher Scientific) was used for.RAW file processing and controlling peptide and protein level false discovery rates, assembling proteins from peptides, and protein quantification from peptides. The MS/MS spectra were searched against a Swissprot human database (January 2021) containing both the forward and reverse sequences. Searches were performed using a 20 ppm precursor mass tolerance, 0.6 Da fragment ion mass tolerance, tryptic peptides containing a maximum of two missed cleavages, static alkylation of cysteine (57.02146 Da), static TMT labelling of lysine residues and N-termini of peptides (229.16293Da), and variable oxidation of methionine (15.99491 Da). TMT reporter ion intensities were measured using a 0.003 Da window around the theoretical m/z for each reporter ion in the MS3 scan. The peptide spectral matches with poor quality MS3 spectra were excluded from quantitation (summed signal-to-noise across channels <100 and precursor isolation specificity <0.5), and the resulting data was filtered to only include proteins with a minimum of 2 unique peptides quantified. Reporter ion intensities were normalized and scaled using in-house scripts in the R framework.[73] Statistical analysis was carried out using the limma package within the R framework.[74]

LFQ quantitative mass spectrometry—Cell pellets were resuspended 8 M urea, 50 mM Tris pH 8.0, 150 mM NaCl, 1 mM β-glycerophosphate, 1 mM NaF, 1 mM sodium orthovanadate, 40 mM NEM and EDTA-free protease inhibitor cocktail (Roche Diagnostics), sonicated, and cleared by centrifugation at 15,000 rpm for 10 min at 4°C. Protein concentrations were determined by BCA Protein assay (Thermo Fisher). 30 μg of each sample was treated with 10 mM TCEP for 10 min, followed by 15 mM iodoacetamide for 10 min. Proteins were precipitated with methanol/chloroform. Precipitated protein was resuspended in 8 M Urea, 50 mM Tris pH 7.8, followed by dilution to 1.85 M urea with the addition of 50 mM Tris pH 7.8. Proteins were digested with LysC for 2 h at 37°C. Samples were diluted two-fold with 50 mM Tris pH 7.8, followed by digestion with trypsin overnight at 37°C. Formic acid/acetonitrile was added to each sample to a final concentration of 1.4%. Samples were desalted using the Stage-Tip method.

Data were collected using a TimsTOF Pro2 (Bruker Daltonics, Bremen, Germany) coupled to a nanoElute LC pump (Bruker Daltonics, Bremen, Germany) via a CaptiveSpray nano-electrospray source. Peptides were separated on a reversed-phase C_{18} column (25 cm × 75 μm ID, 1.6 μM, IonOpticks, Australia) containing an integrated captive spray emitter. Peptides were separated using a 50 min gradient of 2–30% buffer B (acetonitrile in 0.1% formic acid) with a flow rate of 250 nL/min and column temperature maintained at 50°C.

DDA was performed in Parallel Accumulation-Serial Fragmentation (PASEF) mode to determine effective ion mobility windows for downstream diaPASEF data collection.[75] The DDA PASEF parameters included: 100% duty cycle using accumulation and ramp times of 50 ms each, 1 TIMS-MS scan and 10 PASEF ramps per acquisition cycle. The TIMS-MS survey scan was acquired between 100 and 1700 *m/z* and 1/k0 of 0.7–1.3 V s/cm^2. Precursors with 1–5 charges were selected and those that reached an intensity threshold of 20,000 arbitrary units were actively excluded for 0.4 min. The quadrupole isolation width was set to 2 *m/z* for $m/z < 700$ and 3 *m/z* for $m/z > 800$, with the *m/z* between 700 and 800 *m/z* being interpolated linearly. The TIMS elution voltages were calibrated linearly with three points (Agilent ESI-L Tuning Mix Ions; 622, 922, 1,222 *m/z*) to determine the reduced ion mobility coefficients ($1/K_0$). To perform diaPASEF, the precursor distribution in the DDA *m/z*-ion mobility plane was used to design an acquisition scheme for DIA data collection which included two windows in each 50 ms diaPASEF scan. Data was acquired using sixteen of these 25 Da precursor double window scans (creating 32 windows) which covered the diagonal scan line for doubly and triply charged precursors, with singly charged precursors able to be excluded by their position in the m/z-ion mobility plane. These precursor isolation windows were defined between 400 and 1200 *m/z* and 1/k0 of 0.7–1.3 V s/cm^2.

LFQ quantitative LC/MS data analysis and statistical analysis—The diaPASEF raw file processing and controlling peptide and protein level false discovery rates, assembling proteins from peptides, and protein quantification from peptides was performed using library free analysis in DIA-NN 1.8. Library free mode performs an in silico digestion of a given protein sequence database alongside deep learning-based predictions to extract the DIA precursor data into a collection of MS2 spectra. The search results are then used to generate a spectral library which is then employed for the targeted analysis of the

DIA data searched against a Swissprot human database (January 2021). Database search criteria largely followed the default settings for DIA including: tryptic with two missed cleavages, carbomidomethylation of cysteine, and oxidation of methionine and precursor Q-value (FDR) cut-off of 0.01. Precursor quantification strategy was set to Robust LC (high accuracy) with RT-dependent cross run normalization. Proteins with missing values in any of the treatments and with poor quality data were excluded from further analysis (summed abundance across channels of <100 and mean number of precursors used for quantification <2). Protein abundances were scaled using in-house scripts in the R framework[73] and statistical analysis was carried out using the limma package within the R framework.[74]

RNA sequencing and data analysis—Total RNA was extracted using TRIzol (Invitrogen) according to the manufacturer's protocol. After TapeStation analysis to verify sample quality, mRNA stranded libraries were prepared and sequenced on a NovaSeq S4 with PE100. Sequencing reads were aligned to the human genome (BSgenome.Hsapiens.UCSC.hg19, splicedAlignment = FALSE) and quantified at the level of genes (TxDb.Hsapiens.UCSC.hg19.knownGene Bioconductor package) using the QuasR[76] package with default parameters. Differentially expressed Genes were identified using the edgeR Bioconductor package.[77] Differentially expressed genes (DEGs) were used as input to the DAVID Bioinformatics resource.[78,79] Upregulated and downregulated DEGs were separated and used as input into DAVID. Selected genes were assigned a gene ontology biological process designation for the heatmap in Figure 6 based on DAVID. The fold enrichment for selected enriched gene ontology biological process or cytoplasmic component or keyword biological process or domain were plotted. A list of reported NF-κB target genes was collected from https://www.bu.edu/NF-κB/gene-resources/target-genes/and used for determining mRNA abundance changes of known NF-κB targets.

QUANTIFICATION AND STATISTICAL ANALYSIS

Quantification and statistical details can be found in the figure legends.

Supplementary Material

Refer to Web version on PubMed Central for supplementary material.

ACKNOWLEDGMENTS

This work was supported by an American Cancer Society postdoctoral fellowship (PF-19-072-01 - TBE) to J.K.M.; NIH grants R01GM127681 (E.J.B.), R35GM148339 (E.J.B.), and R01CA262188 (E.S.F.); the G. Harold and Leila Y. Mathers Charitable Foundation (E.S.F.); and a Chleck Foundation Fellowship (M.W.M.). This publication includes data generated at the UC San Diego IGM Genomics Center utilizing an Illumina NovaSeq 6000 that was purchased with funding from a National Institutes of Health SIG grant (#S10 OD026929).

DECLARATION OF INTERESTS

E.S.F. is a founder, scientific advisory board (SAB) member, and equity holder of Civetta Therapeutics, Lighthorse Therapeutics, Proximity Therapeutics, and Neomorph, Inc. (board of directors). E.S.F. is an equity holder and SAB member for Avilar Therapeutics and Photys Therapeutics and a consultant to Novartis, Sanofi, EcoR1 Capital, and Deerfield.

The Fischer lab receives or has received research funding from Deerfield, Novartis, Ajax, Interline, Voronoi, and Astellas. K.A.D. is a consultant to Kronos Bio and Neomorph Inc.

INCLUSION AND DIVERSITY

We support inclusive, diverse, and equitable conduct of research.

REFERENCES

1. Yau R, and Rape M. (2016). The increasing complexity of the ubiquitincode. Nat. Cell Biol 18, 579–586. 10.1038/ncb3358. [PubMed: 27230526]
2. Zheng N, and Shabek N. (2017). Ubiquitin ligases: structure, function,and regulation. Annu. Rev. Biochem 86, 129–157. 10.1146/annurev-biochem-060815-014922. [PubMed: 28375744]
3. Harper JW, and Schulman BA (2021). Cullin-RING ubiquitin ligase regulatory circuits: a quarter century beyond the F-box hypothesis. Annu. Rev. Biochem 90, 403–429. 10.1146/annurev-biochem-090120-013613. [PubMed: 33823649]
4. Wang Y, Argiles-Castillo D, Kane EI, Zhou A, and Spratt DE (2020). HECT E3 ubiquitin ligases - emerging insights into their biological roles and disease relevance. J. Cell Sci 133, jcs228072. 10.1242/jcs.228072.
5. Kim JG, Shin HC, Seo T, Nawale L, Han G, Kim BY, Kim SJ,and Cha-Molstad H. (2021). Signaling pathways regulated by UBR box-containing E3 ligases. Int. J. Mol. Sci 22, 8323. 10.3390/ijms22158323. [PubMed: 34361089]
6. Brunet M, Vargas C, Larrieu D, Torrisani J, and Dufresne M. (2020). E3 ubiquitin ligase TRIP12: regulation, structure, and physiopathological functions. Int. J. Mol. Sci 21, 8515. 10.3390/ijms21228515. [PubMed: 33198194]
7. Qi L, Xu X, and Qi X. (2022). The giant E3 ligase HUWE1 is linked totumorigenesis, spermatogenesis, intellectual disability, and inflammatory diseases. Front. Cell. Infect. Microbiol 12, 905906. 10.3389/fcimb.2022.905906.
8. Giles AC, and Grill B. (2020). Roles of the HUWE1 ubiquitin ligase in nervous system development, function and disease. Neural Dev. 15, 6. 10.1186/s13064-020-00143-9. [PubMed: 32336296]
9. Adhikary S, Marinoni F, Hock A, Hulleman E, Popov N, Beier R,Bernard S, Quarto M, Capra M, Goettig S, et al. (2005). The ubiquitin ligase HectH9 regulates transcriptional activation by Myc and is essential for tumor cell proliferation. Cell 123, 409–421. 10.1016/j.cell.2005.08.016. [PubMed: 16269333]
10. Chen D, Kon N, Li M, Zhang W, Qin J, and Gu W. (2005). ARF-BP1/Mule is a critical mediator of the ARF tumor suppressor. Cell 121, 1071–1083. 10.1016/j.cell.2005.03.037. [PubMed: 15989956]
11. Liu Z, Oughtred R, and Wing SS (2005). Characterization of E3Histone, a novel testis ubiquitin protein ligase which ubiquitinates histones. Mol. Cell Biol 25, 2819–2831. 10.1128/MCB.25.7.2819-2831.2005. [PubMed: 15767685]
12. Zhong Q, Gao W, Du F, and Wang X. (2005). Mule/ARF-BP1, a BH3-only E3 ubiquitin ligase, catalyzes the polyubiquitination of Mcl-1 and regulates apoptosis. Cell 121, 1085–1095. 10.1016/j.cell.2005.06.009. [PubMed: 15989957]
13. Hunkeler M, Jin CY, Ma MW, Monda JK, Overwijn D, Bennett EJ, and Fischer ES (2021). Solenoid architecture of HUWE1 contributes to ligase activity and substrate recognition. Mol. Cell 81, 3468–3480.e7. 10.1016/j.molcel.2021.06.032. [PubMed: 34314700]
14. Thompson JW, Nagel J, Hoving S, Gerrits B, Bauer A, Thomas JR, Kirschner MW, Schirle M, and Luchansky SJ (2014). Quantitative Lys–Gly-Gly (diGly) proteomics coupled with inducible RNAi reveals ubiquitin-mediated proteolysis of DNA damage-inducible transcript 4 (DDIT4) by the E3 ligase HUWE1. J. Biol. Chem 289, 28942–28955. 10.1074/jbc.M114.573352. [PubMed: 25147182]

15. Defenouillè re Q, Namane A, Mouaikel J, Jacquier A, and Fromont-Racine M. (2017). The ribosome-bound quality control complex remains associated to aberrant peptides during their proteasomal targeting and interacts with Tom1 to limit protein aggregation. Mol. Biol. Cell 28, 1165–1176. 10.1091/mbc.E16-10-0746. [PubMed: 28298488]

16. Singh RK, Gonzalez M, Kabbaj MHM, and Gunjan A. (2012). NovelE3 ubiquitin ligases that regulate histone protein levels in the budding yeast Saccharomyces cerevisiae. PLoS One 7, e36295. 10.1371/journal.pone.0036295. [PubMed: 22570702]

17. Sung MK, Reitsma JM, Sweredoski MJ, Hess S, and Deshaies RJ (2016). Ribosomal proteins produced in excess are degraded by the ubiquitin-proteasome system. Mol. Biol. Cell 27, 2642–2652. 10.1091/mbc.E16-05-0290. [PubMed: 27385339]

18. Grabarczyk DB, Petrova OA, Deszcz L, Kurzbauer R, Murphy P, Ahel J, Vogel A, Gogova R, Faas V, Kordic D, et al. (2021). HUWE1 employs a giant substrate-binding ring to feed and regulate its HECT E3 domain. Nat. Chem. Biol 17, 1084–1092. 10.1038/s41589-021-00831-5. [PubMed: 34294896]

19. Sun Z, and Brodsky JL (2019). Protein quality control in the secretory pathway. J. Cell Biol 218, 3171–3187. 10.1083/jcb.201906047. [PubMed: 31537714]

20. Atsumi Y, Minakawa Y, Ono M, Dobashi S, Shinohe K, Shinohara A, Takeda S, Takagi M, Takamatsu N, Nakagama H, et al. (2015). ATM and SIRT6/SNF2H mediate transient H2AX stabilization when DSBs form by blocking HUWE1 to allow efficient gammaH2AX foci formation. Cell Rep. 13, 2728–2740. 10.1016/j.celrep.2015.11.054. [PubMed: 26711340]

21. Cassidy KB, Bang S, Kurokawa M, and Gerber SA (2020). Direct regulation of Chk1 protein stability by E3 ubiquitin ligase HUWE1. FEBS J. 287, 1985–1999. 10.1111/febs.15132. [PubMed: 31713291]

22. Choe KN, Nicolae CM, Constantin D, Imamura Kawasawa Y, Delgado-Diaz MR, De S, Freire R, Smits VA, and Moldovan GL (2016). HUWE1 interacts with PCNA to alleviate replication stress. EMBO Rep. 17, 874–886. 10.15252/embr.201541685. [PubMed: 27146073]

23. Dominguez-Brauer C, Hao Z, Elia AJ, Fortin JM, Nechanitzky R, Brauer PM, Sheng Y, Mana MD, Chio IIC, Haight J, et al. (2016). Mule regulates the intestinal stem cell niche via the Wnt pathway and targets EphB3 for proteasomal and lysosomal degradation. Cell Stem Cell 19, 205–216. 10.1016/j.stem.2016.04.002. [PubMed: 27184401]

24. Forget A, Bihannic L, Cigna SM, Lefevre C, Remke M, Barnat M, Dodier S, Shirvani H, Mercier A, Mensah A, et al. (2014). Shh signaling protects Atoh1 from degradation mediated by the E3 ubiquitin ligase Huwe1 in neural precursors. Dev. Cell 29, 649–661. 10.1016/j.devcel.2014.05.014. [PubMed: 24960692]

25. Inoue S, Hao Z, Elia AJ, Cescon D, Zhou L, Silvester J, Snow B, Harris IS, Sasaki M, Li WY, et al. (2013). Mule/Huwe1/Arf-BP1 suppresses Ras-driven tumorigenesis by preventing c-Myc/Miz1-mediated down-regulation of p21 and p15. Genes Dev. 27, 1101–1114. 10.1101/gad.214577.113. [PubMed: 23699408]

26. Mandemaker IK, van Cuijk L, Janssens RC, Lans H, Bezstarosti K, Hoeijmakers JH, Demmers JA, Vermeulen W, and Marteijn JA (2017). DNA damage-induced histone H1 ubiquitylation is mediated by HUWE1 and stimulates the RNF8-RNF168 pathway. Sci. Rep 7, 15353. 10.1038/s41598-017-15194-y. [PubMed: 29127375]

27. Parsons JL, Tait PS, Finch D, Dianova II, Edelmann MJ, Khoronenkova SV, Kessler BM, Sharma RA, McKenna WG, and Dianov GL (2009). Ubiquitin ligase ARF-BP1/Mule modulates base excision repair. EMBO J. 28, 3207–3215. 10.1038/emboj.2009.243. [PubMed: 19713937]

28. Wang X, Lu G, Li L, Yi J, Yan K, Wang Y, Zhu B, Kuang J, Lin M, Zhang S, and Shao G. (2014). HUWE1 interacts with BRCA1 and promotes its degradation in the ubiquitin-proteasome pathway. Biochem. Biophys. Res. Commun 444, 549–554. 10.1016/j.bbrc.2014.01.075. [PubMed: 24472556]

29. Zhao X, D' Arca D, Lim WK, Brahmachary M, Carro MS, Ludwig T,Cardo CC, Guillemot F, Aldape K, Califano A, et al. (2009). The N-Myc-DLL3 cascade is suppressed by the ubiquitin ligase Huwe1 to inhibit proliferation and promote neurogenesis in the developing brain. Dev. Cell 17, 210–221. 10.1016/j.devcel.2009.07.009. [PubMed: 19686682]

30. Zhao X, Heng JIT, Guardavaccaro D, Jiang R, Pagano M, Guillemot F, Iavarone A, and Lasorella A. (2008). The HECT-domain ubiquitin ligase Huwe1 controls neural differentiation

and proliferation by destabilizing the N-Myc oncoprotein. Nat. Cell Biol 10, 643–653. 10.1038/ncb1727. [PubMed: 18488021]

31. Endres T, Solvie D, Heidelberger JB, Andrioletti V, Baluapuri A, Ade CP, Muhar M, Eilers U, Vos SM, Cramer P, et al. (2021). Ubiquitylation of MYC couples transcription elongation with double-strand break repair at active promoters. Mol. Cell 81, 830–844.e13. 10.1016/j.molcel.2020.12.035. [PubMed: 33453168]
32. Hao Z, Duncan GS, Su YW, Li WY, Silvester J, Hong C, You H, Brenner D, Gorrini C, Haight J, et al. (2012). The E3 ubiquitin ligase Mule acts through the ATM-p53 axis to maintain B lymphocyte homeostasis. J. Exp. Med 209, 173–186. 10.1084/jem.20111363. [PubMed: 22213803]
33. King B, Boccalatte F, Moran-Crusio K, Wolf E, Wang J, Kayembe C, Lazaris C, Yu X, Aranda-Orgilles B, Lasorella A, and Aifantis I. (2016). The ubiquitin ligase Huwe1 regulates the maintenance and lymphoid commitment of hematopoietic stem cells. Nat. Immunol 17, 1312–1321. 10.1038/ni.3559. [PubMed: 27668798]
34. Kon N, Zhong J, Qiang L, Accili D, and Gu W. (2012). Inactivation of arf-bp1 induces p53 activation and diabetic phenotypes in mice. J. Biol. Chem 287, 5102–5111. 10.1074/jbc.M111.322867. [PubMed: 22187431]
35. Myant KB, Cammareri P, Hodder MC, Wills J, Von Kriegsheim A, Győrffy B, Rashid M, Polo S, Maspero E, Vaughan L, et al. (2017). HUWE1 is a critical colonic tumour suppressor gene that prevents MYC signalling, DNA damage accumulation and tumour initiation. EMBO Mol. Med 9, 181–197. 10.15252/emmm.201606684.
36. Peter S, Bultinck J, Myant K, Jaenicke LA, Walz S, Müller J, Gmachl M, Treu M, Boehmelt G, Ade CP, et al. (2014). Tumor cell-specific inhibition of MYC function using small molecule inhibitors of the HUWE1 ubiquitin ligase. EMBO Mol. Med 6, 1525–1541. 10.15252/emmm.201403927.
37. Yang D, Cheng D, Tu Q, Yang H, Sun B, Yan L, Dai H, Luo J, Mao B, Cao Y, et al. (2018). HUWE1 controls the development of non-small cell lung cancer through down-regulation of p53. Theranostics 8, 3517–3529. 10.7150/thno.24401.
38. Kunz V, Bommert KS, Kruk J, Schwinning D, Chatterjee M,Stühmer T, Bargou R, and Bommert K. (2020). Targeting of the E3 ubiquitin-protein ligase HUWE1 impairs DNA repair capacity and tumor growth in preclinical multiple myeloma models. Sci. Rep 10, 18419. 10.1038/s41598-020-75499-3. [PubMed: 33116152]
39. Markkanen E, van Loon B, Ferrari E, Parsons JL, Dianov GL, and Hübscher U. (2012). Regulation of oxidative DNA damage repair by DNA polymerase lambda and MutYH by cross-talk of phosphorylation and ubiquitination. Proc. Natl. Acad. Sci. USA 109, 437–442. 10.1073/pnas.1110449109. [PubMed: 22203964]
40. Froyen G, Belet S, Martinez F, Santos-Rebouç as CB, Declercq M, Verbeeck J, Donckers L, Berland S, Mayo S/M, et al. (2012). Copy-number gains of HUWE1 due to replication- and recombination-based rearrangements. Am. J. Hum. Genet 91, 252–264. 10.1016/j.ajhg.2012.06.010. [PubMed: 22840365]
41. Madrigal I, Rodríguez-Revenga L, Armengol L, González E, Rodriguez B, Badenas C, Sánchez A, Martıńez F, Guitart M, Fernández I, et al. (2007). X-chromosome tiling path array detection of copy number variants in patients with chromosome X-linked mental retardation. BMC Genom. 8, 443. 10.1186/1471-2164-8-443.
42. Froyen G, Corbett M, Vandewalle J, Jarvela I, Lawrence O, Meldrum C, Bauters M, Govaerts K, Vandeleur L, Van Esch H, et al. (2008). Submicroscopic duplications of the hydroxysteroid dehydrogenase HSD17B10 and the E3 ubiquitin ligase HUWE1 are associated with mental retardation. Am. J. Hum. Genet 82, 432–443. 10.1016/j.ajhg.2007.11.002. [PubMed: 18252223]
43. Hundley FV, Sanvisens Delgado N, Marin HC, Carr KL, Tian R, and Toczyski DP (2021). A comprehensive phenotypic CRISPR-Cas9 screen of the ubiquitin pathway uncovers roles of ubiquitin ligases in mitosis. Mol. Cell 81, 1319–1336.e9. 10.1016/j.molcel.2021.01.014. [PubMed: 33539788]
44. Hein MY, Hubner NC, Poser I, Cox J, Nagaraj N, Toyoda Y, Gak IA, Weisswange I, Mansfeld J, Buchholz F, et al. (2015). A human interactome in three quantitative dimensions organized by stoichiometries and abundances. Cell 163, 712–723. 10.1016/j.cell.2015.09.053. [PubMed: 26496610]

45. Vazquez F, and Boehm JS (2020). The Cancer Dependency Map enables drug mechanism-of-action investigations. Mol. Syst. Biol 16, e9757. 10.15252/msb.20209757. [PubMed: 32696566]
46. Amici DR, Ansel DJ, Metz KA, Smith RS, Phoumyvong CM, Gayatri S, Chamera T, Edwards SL, O'Hara BP, Srivastava S, et al. (2022). C16orf72/HAPSTR1 is a molecular rheostat in an integrated network of stress response pathways. Proc. Natl. Acad. Sci. USA 119, e2111262119. 10.1073/pnas.2111262119.
47. Behan FM, Iorio F, Picco G, Gonç alves, E., Beaver, C.M., Migliardi, G., Santos, R., Rao, Y., Sassi, F., Pinnelli, M., et al. (2019). Prioritization of cancer therapeutic targets using CRISPR-Cas9 screens. Nature 568, 511–516. 10.1038/s41586-019-1103-9. [PubMed: 30971826]
48. Dempster JM, Pacini C, Pantel S, Behan FM, Green T, Krill-Burger J, Beaver CM, Younger ST, Zhivich V, Najgebauer H, et al. (2019). Agreement between two large pan-cancer CRISPR-Cas9 gene dependency data sets. Nat. Commun 10, 5817. 10.1038/s41467-019-13805-y. [PubMed: 31862961]
49. Benslimane Y, Sá nchez-Osuna, Coulombe-Huntington J, Bertomeu T, Henry D, Huard C, Bonneil É, Thibault P, Tyers M, and Harrington L. (2021). A novel p53 regulator, C16ORF72/TAPR1, buffers against telomerase inhibition. Aging Cell 20, e13331. 10.1111/acel.13331.
50. Tai HC, Besche H, Goldberg AL, and Schuman EM (2010). Characterization of the brain 26S proteasome and its interacting proteins. Front. Mol. Neurosci 3, 12. 10.3389/fnmol.2010.00012. [PubMed: 20717473]
51. Thul PJ, Åkesson L, Wiking M, Mahdessian D, Geladaki A, Ait Blal H, Alm T, Asplund A, Björk L, Breckels LM, et al. (2017). A subcellular map of the human proteome. Science 356, eaal3321. 10.1126/science.aal3321.
52. Uhlé n M., Fagerberg L, Hallström BM, Lindskog C, Oksvold P, Mardinoglu A, Sivertsson Å, Kampf C, Sjöstedt E, Asplund A, et al. (2015). Proteomics. Tissue-based map of the human proteome. Science 347, 1260419. 10.1126/science.1260419.
53. Nusinow DP, Szpyt J, Ghandi M, Rose CM, McDonald ER 3rd, Kalocsay M, Jané-Valbuena J, Gelfand E, Schweppe DK, Jedrychowski M, et al. (2020). Quantitative proteomics of the cancer cell line encyclopedia. Cell 180, 387–402.e16. 10.1016/j.cell.2019.12.023. [PubMed: 31978347]
54. Roider HG, Manke T, O'Keeffe S, Vingron M, and Haas SA (2009). PASTAA: identifying transcription factors associated with sets of co-regulated genes. Bioinformatics 25, 435–442. 10.1093/bioinformatics/btn627. [PubMed: 19073590]
55. Zhou W, Pal AS, Hsu AYH, Gurol T, Zhu X, Wirbisky-Hershberger SE, Freeman JL, Kasinski AL, and Deng Q. (2018). MicroRNA-223 suppresses the canonical NF-kappaB pathway in basal keratinocytes to dampen neutrophilic inflammation. Cell Rep. 22, 1810–1823. 10.1016/j.celrep.2018.01.058. [PubMed: 29444433]
56. Ohtake F, Saeki Y, Ishido S, Kanno J, and Tanaka K. (2016). The K48-K63 branched ubiquitin chain regulates NF-kappaB signaling. Mol. Cell 64, 251–266. 10.1016/j.molcel.2016.09.014. [PubMed: 27746020]
57. Gong X, Du D, Deng Y, Zhou Y, Sun L, and Yuan S. (2020). The structure and regulation of the E3 ubiquitin ligase HUWE1 and its biological functions in cancer. Invest. New Drugs 38, 515–524. 10.1007/s10637-020-00894-6. [PubMed: 32008177]
58. Opperman KJ, Mulcahy B, Giles AC, Risley MG, Birnbaum RL, Tulgren ED, Dawson-Scully K, Zhen M, and Grill B. (2017). The HECT family ubiquitin ligase EEL-1 regulates neuronal function and development. Cell Rep. 19, 822–835. 10.1016/j.celrep.2017.04.003. [PubMed: 28445732]
59. Kats I, Reinbold C, Kschonsak M, Khmelinskii A, Armbruster L, Ruppert T, and Knop M. (2022). Up-regulation of ubiquitin-proteasome activity upon loss of NatA-dependent N-terminal acetylation. Life Sci. Alliance 5, e202000730. 10.26508/lsa.202000730.
60. Poulsen EG, Steinhauer C, Lees M, Lauridsen AM, Ellgaard L, and Hartmann-Petersen R. (2012). HUWE1 and TRIP12 collaborate in degradation of ubiquitin-fusion proteins and misframed ubiquitin. PLoS One 7, e50548. 10.1371/journal.pone.0050548. [PubMed: 23209776]
61. Yau RG, Doerner K, Castellanos ER, Haakonsen DL, Werner A, Wang N, Yang XW, Martinez-Martin N, Matsumoto ML, Dixit VM, and Rape M. (2017). Assembly and function of heterotypic ubiquitin chains in cell-cycle and protein quality control. Cell 171, 918–933.e20. 10.1016/j.cell.2017.09.040. [PubMed: 29033132]

62. Kolla S, Ye M, Mark KG, and Rapé M. (2022). Assembly and function of branched ubiquitin chains. Trends Biochem. Sci 47, 759–771. 10.1016/j.tibs.2022.04.003. [PubMed: 35508449]
63. Kaiho-Soma A, Akizuki Y, Igarashi K, Endo A, Shoda T, Kawase Y, Demizu Y, Naito M, Saeki Y, Tanaka K, and Ohtake F. (2021). TRIP12 promotes small-molecule-induced degradation through K29/K48-branched ubiquitin chains. Mol. Cell 81, 1411–1424.e7. 10.1016/j.molcel.2021.01.023. [PubMed: 33567268]
64. Johnson AG, Flynn RA, Lapointe CP, Ooi YS, Zhao ML, Richards CM, Qiao W, Yamada SB, Couthouis J, Gitler AD, et al. (2020). A memory of eS25 loss drives resistance phenotypes. Nucleic Acids Res. 48, 7279–7297. 10.1093/nar/gkaa444. [PubMed: 32463448]
65. Meerbrey KL, Hu G, Kessler JD, Roarty K, Li MZ, Fang JE, Herschkowitz JI, Burrows AE, Ciccia A, Sun T, et al. (2011). The pINDUCER lentiviral toolkit for inducible RNA interference in vitro and in vivo. Proc. Natl. Acad. Sci. USA 108, 3665–3670. 10.1073/pnas.1019736108. [PubMed: 21307310]
66. Yang X, Boehm JS, Yang X, Salehi-Ashtiani K, Hao T, Shen Y, Lubonja R, Thomas SR, Alkan O, Bhimdi T, et al. (2011). A public genome-scale lentiviral expression library of human ORFs. Nat. Methods 8, 659–661. 10.1038/nmeth.1638. [PubMed: 21706014]
67. Abdulrahman W, Uhring M, Kolb-Cheynel I, Garnier JM, Moras D, Rochel N, Busso D, and Poterszman A. (2009). A set of baculovirus transfer vectors for screening of affinity tags and parallel expression strategies. Anal. Biochem 385, 383–385. 10.1016/j.ab.2008.10.044. [PubMed: 19061853]
68. Luo Y, Hara T, Ishido Y, Yoshihara A, Oda K, Makino M, Ishii N, Hiroi N, and Suzuki K. (2014). Rapid preparation of high-purity nuclear proteins from a small number of cultured cells for use in electrophoretic mobility shift assays. BMC Immunol. 15, 586. 10.1186/s12865-014-0062-z. [PubMed: 25527077]
69. Schindelin J, Arganda-Carreras I, Frise E, Kaynig V, Longair M, Pietzsch T, Preibisch S, Rueden C, Saalfeld S, Schmid B, et al. (2012). Fiji: an open-source platform for biological-image analysis. Nat. Methods 9, 676–682. 10.1038/Nmeth.2019. [PubMed: 22743772]
70. Stirling DR, Swain-Bowden MJ, Lucas AM, Carpenter AE, Cimini BA, and Goodman A. (2021). CellProfiler 4: improvements in speed, utility and usability. BMC Bioinformatics 22, 433. 10.1186/s12859-021-04344-9. [PubMed: 34507520]
71. Donovan KA, An J, Nowak RP, Yuan JC, Fink EC, Berry BC, Ebert BL, and Fischer ES (2018). Thalidomide promotes degradation of SALL4, a transcription factor implicated in Duane Radial Ray syndrome. Elife 7, e38430. 10.7554/eLife.38430. [PubMed: 30067223]
72. McAlister GC, Nusinow DP, Jedrychowski MP, Wuhr M, Huttlin EL, Erickson BK, Rad R, Haas W, and Gygi SP. (2014). MultiNotch MS3 enables accurate, sensitive, and multiplexed detection of differential expression across cancer cell line proteomes. Anal. Chem 86, 7150–7158. 10.1021/ac502040v. [PubMed: 24927332]
73. R Core Team (2014). R: A Language and Environment for Statistical Computing (R Foundation for Statistical Computing).
74. Ritchie ME, Phipson B, Wu D, Hu Y, Law CW, Shi W, and Smyth GK (2015). Limma powers differential expression analyses for RNA-sequencing and microarray studies. Nucleic Acids Res. 43, e47. 10.1093/nar/gkv007. [PubMed: 25605792]
75. Meier F, Brunner A-D, Frank M, Ha A, Bludau I, Voytik E, Kaspar-Schoenefeld S, Lubeck M, Raether O, Bache N, et al. (2020). diaPASEF: parallel accumulation–serial fragmentation combined with data-independent acquisition. Nat. Methods 17, 1229–1236. [PubMed: 33257825]
76. Gaidatzis D, Lerch A, Hahne F, and Stadler MB (2015). QuasR: quantification and annotation of short reads in R. Bioinformatics 31, 1130–1132. 10.1093/bioinformatics/btu781. [PubMed: 25417205]
77. Robinson MD, McCarthy DJ, and Smyth GK (2010). edgeR: a Bioconductor package for differential expression analysis of digital gene expression data. Bioinformatics 26, 139–140. 10.1093/bioinformatics/btp616. [PubMed: 19910308]
78. Huang DW, Sherman BT, and Lempicki RA (2009). Bioinformatics enrichment tools: paths toward the comprehensive functional analysis of large gene lists. Nucleic Acids Res. 37, 1–13. 10.1093/nar/gkn923. [PubMed: 19033363]

79. Huang DW, Sherman BT, and Lempicki RA (2009). Systematic and integrative analysis of large gene lists using DAVID bioinformatics resources. Nat. Protoc 4, 44–57. 10.1038/nprot.2008.211. [PubMed: 19131956]

Highlights

- HUWE1 substrates are diverse and largely cell-type specific
- HAPSTR1/C16orf72 is a HUWE1 substrate in multiple cell lines
- HAPSTR1 localizes HUWE1 to the nucleus
- Nuclear HUWE1 is required for cell proliferation and modulates p53 and NF-κB pathways

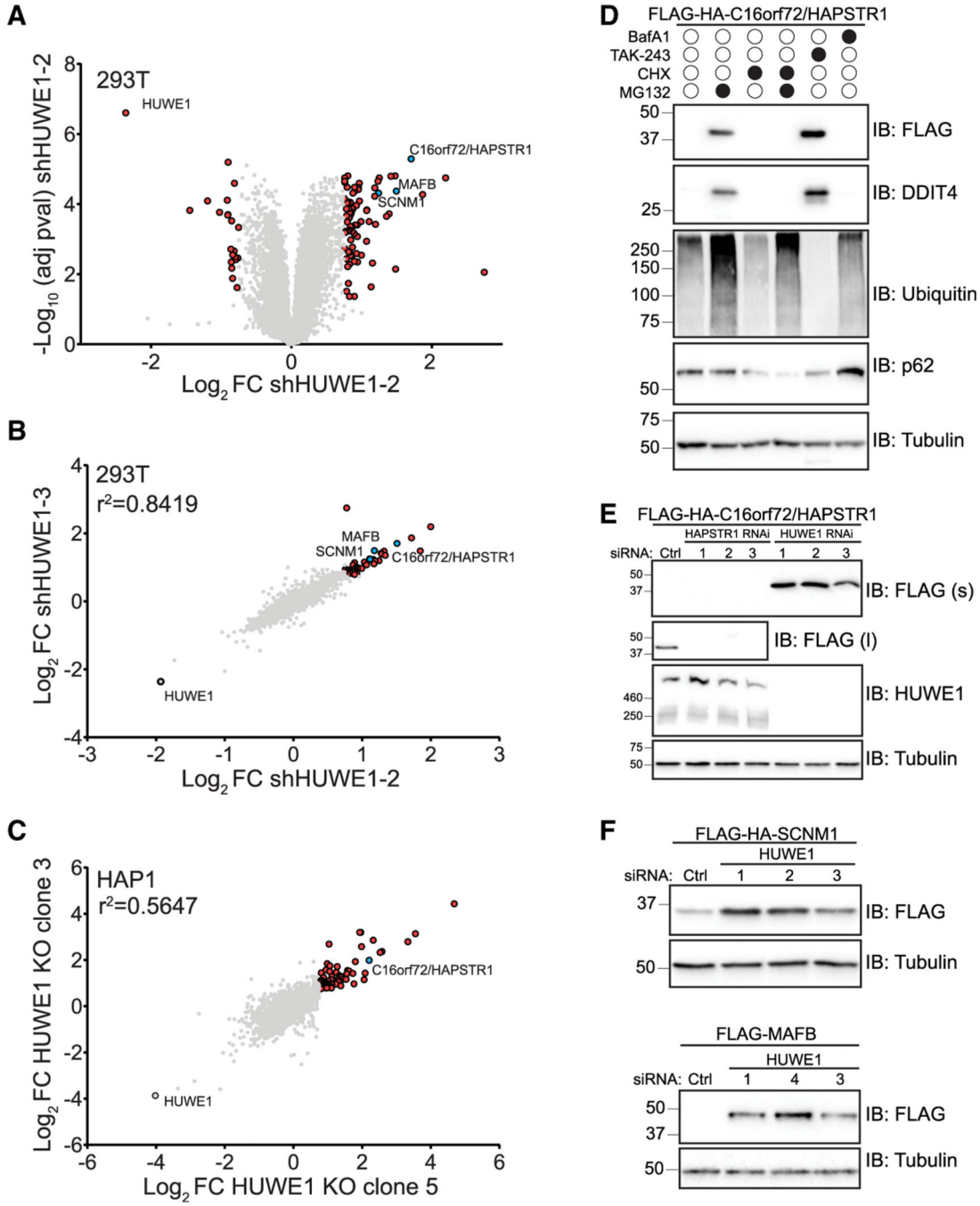

Figure 1. Identification of HUWE1 substrates using quantitative proteomics

(A) Volcano plot depicting the $\log_2$ fold change (FC) and $\log_{10}$ p value for quantified proteins in 293T cells after doxycycline-inducible expression of an shRNA targeting HUWE1 relative to a firefly luciferase knockdown. Proteins with altered abundance in response to HUWE1 knockdown are indicated in red. Proteins selected for further analysis are indicated in blue.

(B) Scatterplot comparing the $\log_2$ FC for all quantified proteins in 293T cells after doxycycline-inducible expression of two different shRNAs targeting HUWE1 relative to

a firefly luciferase knockdown. Proteins with altered abundance in response to HUWE1 knockdown are indicated in red. Proteins selected for further analysis are indicated in blue.
(C) Scatterplot comparing the $\log_2$ FC for all quantified proteins quantified in two HUWE1 knockout (KO) clones of HAP1 cells. Proteins with altered abundance in response to HUWE1 knockdown are indicated in red. Proteins selected for further analysis are indicated in blue.
(D) Immunoblots of 293T cells stably expressing FLAG-HA-tagged C16orf72/HAPSTR1 were treated with bafilomycin A1 (BafA1), TAK-243, cycloheximide (CHX), or MG132 for 8 h. Whole-cell extracts were separated by SDS-PAGE and immunoblotted (IB) with the indicated antibodies.
(E) Immunoblots of 293T cells stably expressing FLAG-HA-tagged C16orf72/HAPSTR1 and transfected with a control (Ctrl) siRNA or one of three C16orf72/HAPSTR1 or HUWE1 targeting siRNAs. Whole-cell extracts were separated by SDS-PAGE and IB with the indicated antibodies (s, short exposure; l, long exposure).
(F) Immunoblots of 293T cells stably expressing FLAG-HA-tagged SCNM1 (top) or transiently transfected with FLAG-tagged MAFB (bottom) and transfected with a control (Ctrl) siRNA or one of three HUWE1 targeting siRNAs. Whole-cell extracts were separated by SDS-PAGE and IB with the indicated antibodies.
See also Figure S1 and Tables S1, S2, and S3.

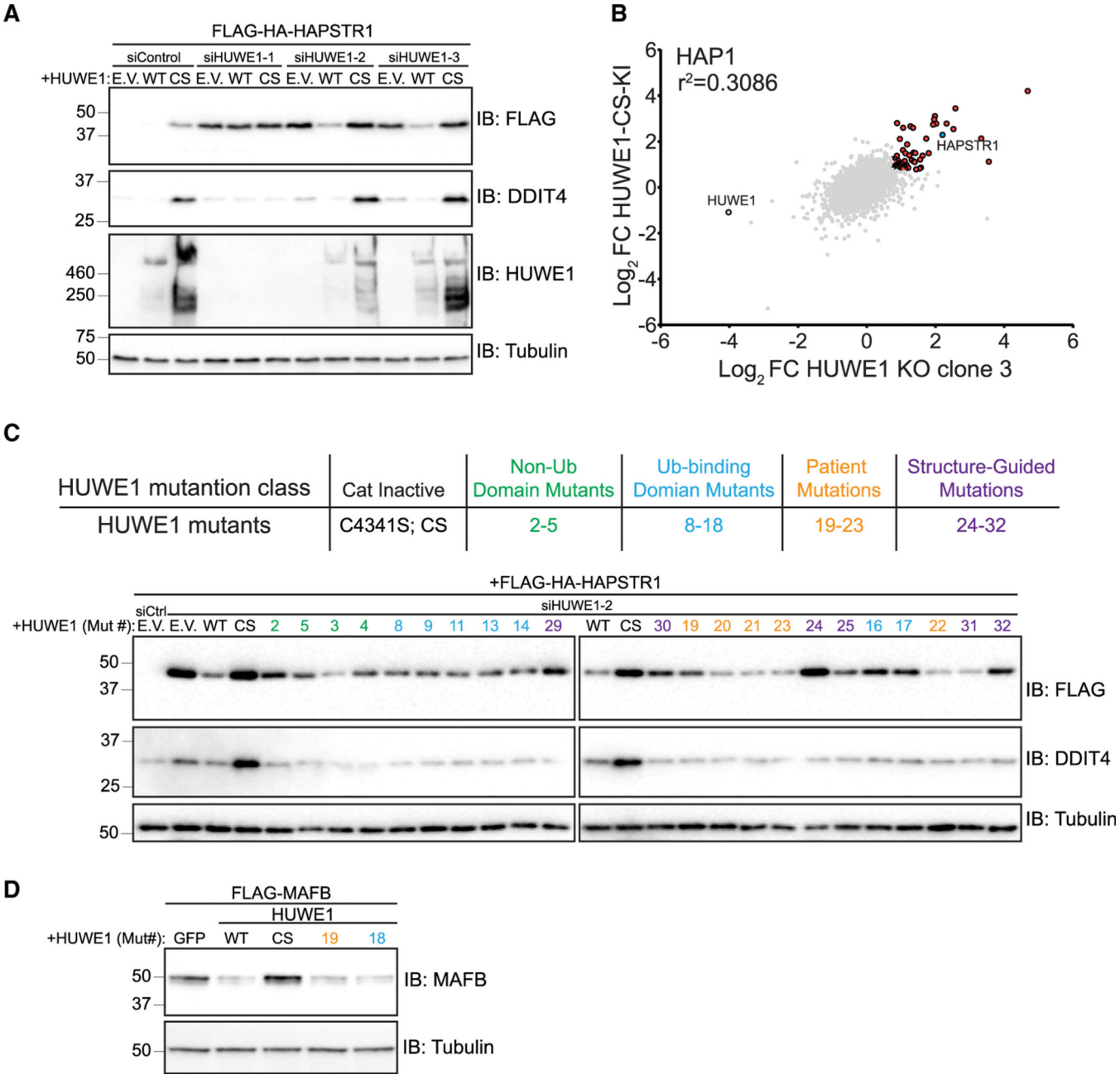

Figure 2. HAPSTR1 is a HUWE1 substrate

(A) Immunoblots of 293T cells stably expressing FLAG-HA-tagged HAPSTR1 and co-transfected with a control or HUWE1 targeting siRNA and either an emptyvector (E.V.) control, WT HUWE1, or HUWE1 C4341S (CS). The HUWE1 transgenes are resistant to siHUWE1–2 and siHUWE1–3. Whole-cell extracts were separated by SDS-PAGE and IB with the indicated antibodies.

(B) Scatterplot comparing the $\log_2$ FC for all quantified proteins in a HUWE1 KO HAP1 clone and a HUWE1 CS knockin (KI) HAP1 clone. Proteins whose abundance is significantly elevated in both cell lines are shown in red. Proteins selected for further analysis are indicated in blue.

(C) Immunoblots of 293T cells stably expressing FLAG-HA-tagged HAPSTR1 and co-transfected with a control (siCtrl) or HUWE1-targeting siRNA and either anempty vector (E.V.) control or the indicated variant of siRNA-resistant HUWE1. Whole-cell extracts were separated by SDS-PAGE and IB with the indicated antibodies.
(D) Immunoblots of 293T cells transiently transfected with FLAG–tagged MAFB and either a GFP control or the indicated HUWE1 variant. Variants labeled as in(C). Whole-cell extracts were separated by SDS-PAGE and IB with the indicated antibodies.
See also Figure S2 and Table S4.

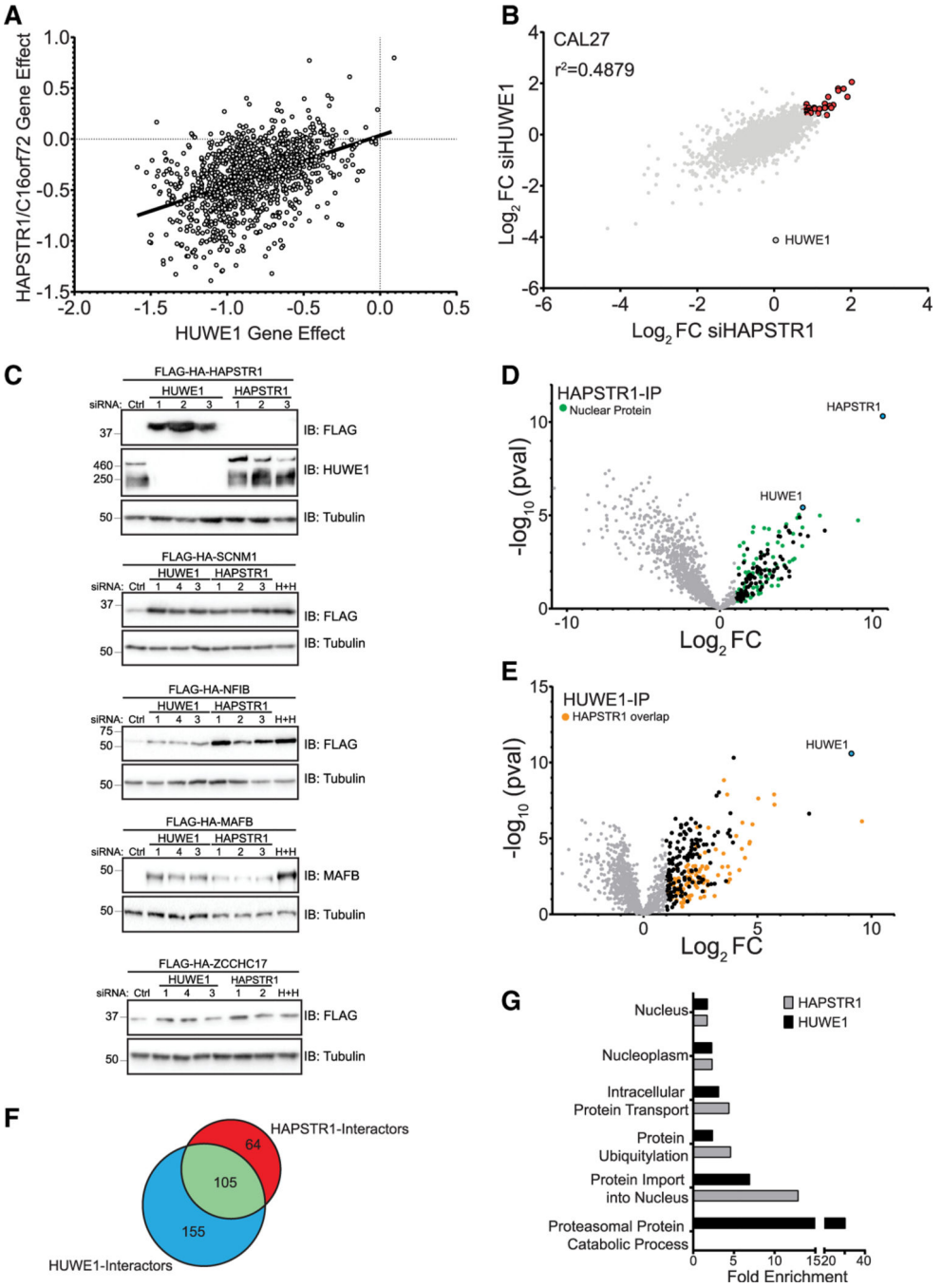

Figure 3. HAPSTR1 assists HUWE1 in targeting nuclear substrates

(A) Scatterplot of DepMap 22Q2 CRISPR gene effect scores for HUWE1 and C16orf72/HAPSTR1. The solid line depicts the best-fit line using linear regression.

(B) Scatterplot comparing the $\log_2$ FC for all quantified proteins in CAL27 cells after transfection of a HUWE1- or HAPSTR1-targeting siRNA relative to a control siRNA. Proteins with increased abundance in both HUWE1 and HAPSTR1 knockdown cells are indicated in red.

(C) Immunoblots of CAL27 cells stably expressing the indicated FLAG-HA-tagged transgene and transfected with siRNA. H + H indicates combined HUWE1 and HAPSTR1 knockdown. Whole-cell extracts were separated by SDS-PAGE and IB with the indicated antibodies.

(D) Volcano plot depicting the $\log_2$ FC and _$\log_{10}$ p value for proteins identified by mass spectrometry in HAPSTR1 immune complexes compared with control immunoprecipitations. Proteins that are significantly enriched with HAPSTR1 are shown as black dots. Significantly enriched proteins with reported nuclear localization are shown as green dots.

(E) Volcano plot depicting the $\log_2$ FC and _$\log_{10}$ p value for proteins identified by mass spectrometry in HUWE1 immune complexes compared with control immunoprecipitations. Proteins that are significantly enriched with HUWE1 are shown as black dots. HUWE1-interacting proteins that are also enriched with HAPSTR1 are depicted as orange dots.

(F) Overlap of identified HUWE1- and HAPSTR1-interacting proteins.

(G) Fold enrichment of indicated Gene Ontology terms associated with HUWE1- or HAPSTR1-interacting proteins.

See also Figure S3 and Tables S5 and S6.

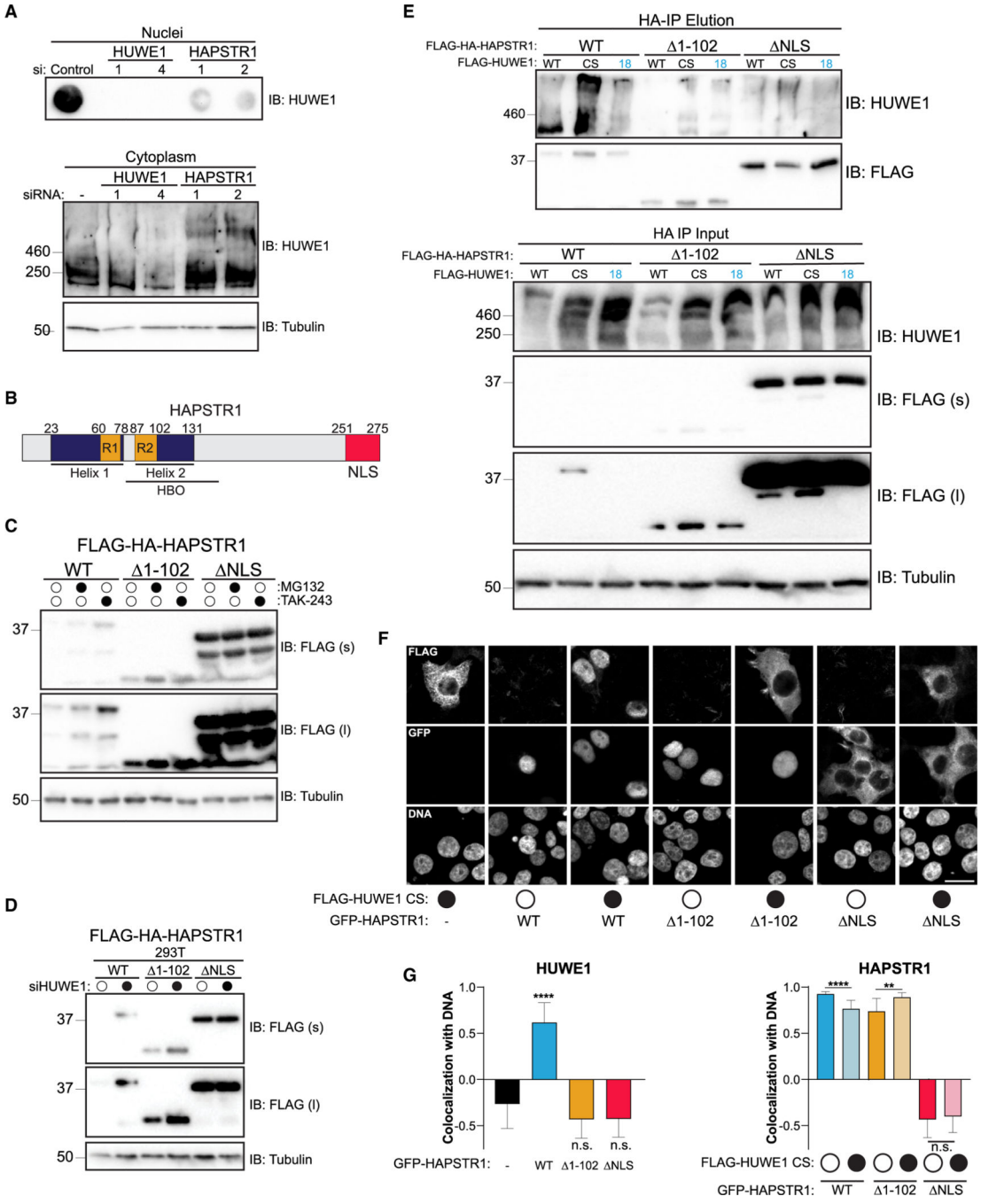

Figure 4. HUWE1 nuclear localization requires HAPSTR1

(A) Immunoblots of NCI-H2052 cells transfected with a control siRNA or one of two siRNA sequences targeting either HUWE1 or HAPSTR1. (Top) The nuclei were isolated and analyzed by dot blot. (Bottom) The cytoplasmic fractions were separated by SDS-PAGE. IB was performed with the indicated antibodies.

(B) Schematic of HAPSTR1 protein sequence features. Predicted α helices are shown in purple, conserved repeated regions in orange, and an NLS in red. (C) Immunoblots of 293T cells stably expressing FLAG-HA-tagged WT or the indicated variant of HAPSTR1 treated

with MG132 or TAK-243. Whole-cell extracts were separated by SDS-PAGE and IB with the indicated antibodies.

(D) Immunoblots of 293T cells stably expressing siRNA-resistant FLAG-HA-tagged WT or the indicated variant of HAPSTR1 transfected with a control or HUWE-1targeting siRNA. Whole-cell extracts were separated by SDS-PAGE and IB with the indicated antibodies (s, short exposure; l, long exposure).

(E) Immunoblots of HA immunoprecipitations (top) and inputs (bottom) from 293T cells stably expressing FLAG-HA-tagged WT or the indicated variant ofHAPSTR1 and transfected with the indicated FLAG–tagged HUWE1 variant. Samples were separated by SDS-PAGE and IB with the indicated antibodies (s, short exposure; l, long exposure).

(F) Immunofluorescence images of 293T cells transfected with FLAG-tagged HUWE1 CS alone or in combination with the indicated GFP-tagged HAPSTR1. Scalebar, 20 μm.

(G) Quantification of the colocalization of DNA and HUWE1 (left) or HAPSTR1 (right). Data are represented as the mean + SD for all cells quantified ($11 \leq n \geq 51$). Analysis included cells from at least two biological replicates for all conditions. Statistical significance was determined by Kolmogorov-Smirnov t test. ****$p \leq 0.0001$; **$p \leq 0.01$; n.s., $p > 0.05$.

See also Figure S4.

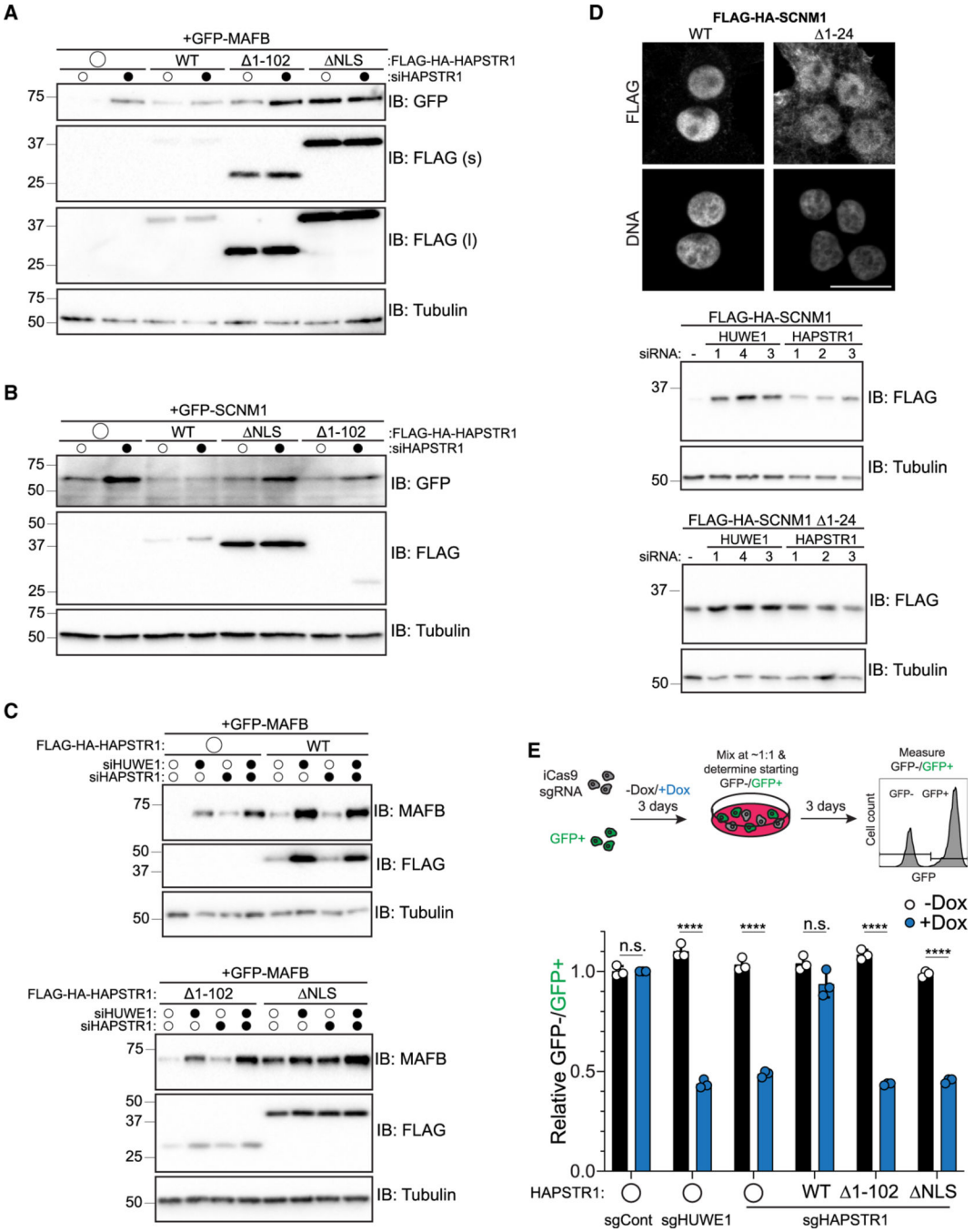

Figure 5. Loss of nuclear HUWE1 stabilizes nuclear targets and reduces cellular proliferation

(A) Immunoblots of 293T cells stably expressing the indicated siRNA-resistant FLAG-HA-tagged HAPSTR1 variant and transfected with GFP-tagged MAFB and acontrol or HAPSTR1-targeting siRNA. Whole-cell extracts were separated by SDS-PAGE and IB with the indicated antibodies (s, short exposure; l, long exposure).

(B) Immunoblots of CAL27 cells stably expressing GFP-SCNM1 and the indicated variant of siRNA-resistant FLAG-HA-tagged HAPSTR1 and transfected with acontrol or

HAPSTR1-targeting siRNA. Whole-cell extracts were separated by SDS-PAGE and IB with the indicated antibodies.

(C) Immunoblots of 293T cells stably expressing the indicated siRNA-resistant FLAG-HA-tagged HAPSTR1 variant and transfected with GFP-tagged MAFB andthe indicated siRNA. Whole-cell extracts were separated by SDS-PAGE and IB with the indicated antibodies (s, short exposure; l, long exposure).

(D) CAL27 cells stably expressing the indicated FLAG-HA-SCNM1 variant were generated. (Top) Immunofluorescence images. Scale bar, 20 μm. (Bottom) Immunoblots after transfection with the indicated siRNA. Whole-cell extracts were separated by SDS-PAGE and IB with the indicated antibodies.

(E) (Top) Schematic of the CRISPR-Cas9-based competitive growth assay. (Bottom) CAL27 cells expressing inducible Cas9, the indicated sgRNA, and the indicated sgRNA-resistant HAPSTR1 variant were treated with doxycycline for 3 days prior to co-culturing with GFP+ CAL27 cells. The relative GFP−:GFP+ ratio of the population was measured 3 days after co-culture. Data are represented as the mean ± SD of three replicates. Statistical significance was determined by unpaired t test. ****$p \leq 0.0001$; n.s., $p > 0.05$.

See also Figure S5.

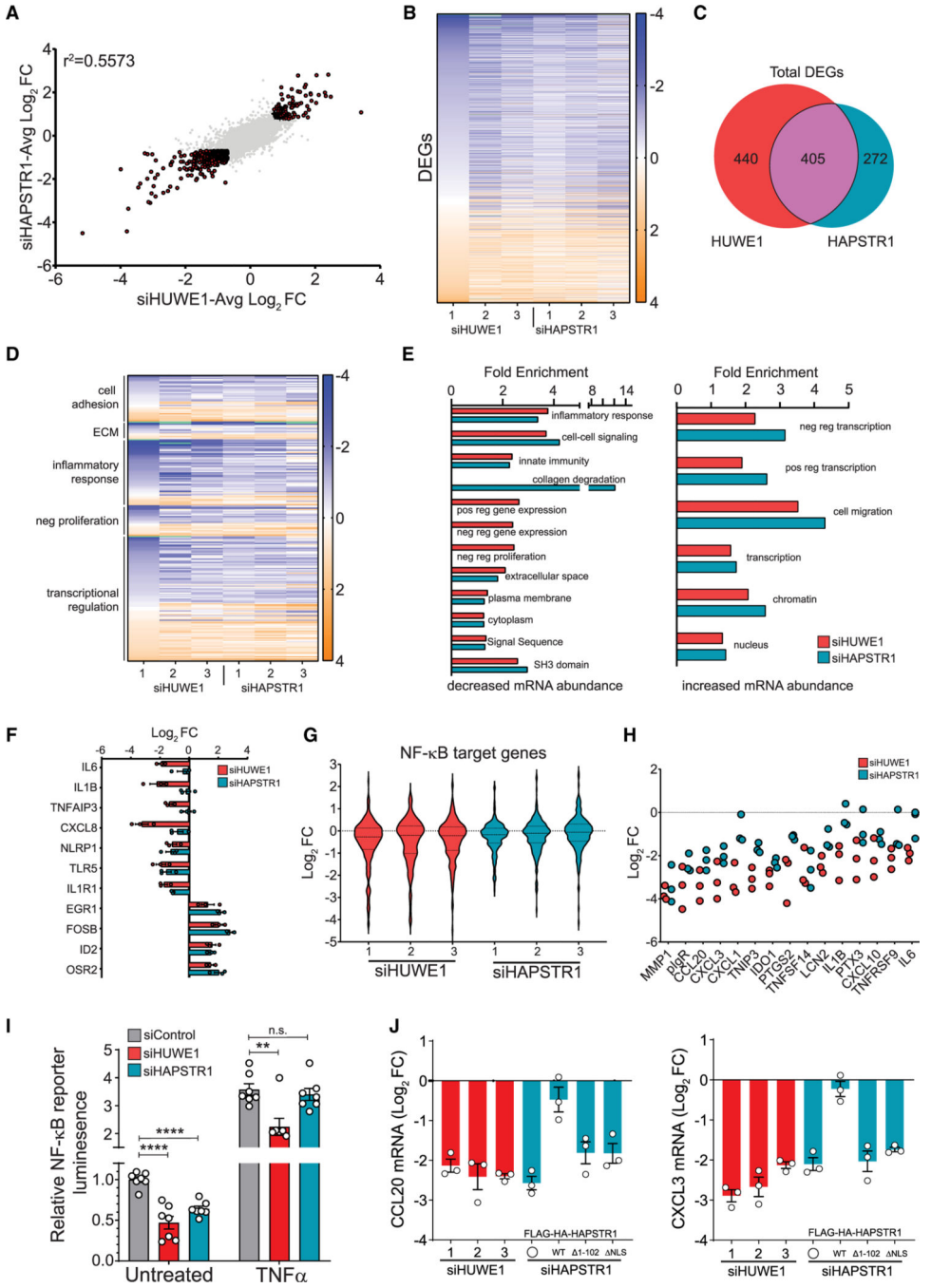

Figure 6. HAPSTR1 and HUWE1 regulate overlapping transcriptional programs

(A) Scatterplot comparing the $\log_2$ FC for all mRNA quantified by RNA-seq in CAL27 cells after transfection of a HUWE1- or HAPSTR1-targeting siRNA relative to a control siRNA. The data represent the average across three different siRNA sequences targeting HUWE1 and HAPSTR1. Differentially expressed genes in both HUWE1 and HAPSTR1 knockdown cells are indicated in red.

(B) Heatmap of the differentially expressed genes after HUWE1 or HAPSTR1 knockdown in CAL27 cells. Color map indicates $\log_2$ FC.

(C) Venn diagram of the differentially expressed genes after HUWE1 or HAPSTR1 knockdown in CAL27 cells.
(D) Heatmap of a subset of differentially expressed genes after HUWE1 or HAPSTR1 knockdown in CAL27 cells clustered by selected enriched Gene Ontology terms.
(E) Selected enriched Gene Ontology biological processes, cellular components, or pfam domains of mRNAs with decreased abundance (left) or increased abundance (right) in CAL27 cells after HUWE1 or HAPSTR1 knockdown.
(F) The $\log_2$ FC of selected inflammatory or transcriptional regulation genes in CAL27 cells after HUWE1 or HAPSTR1 knockdown. N = 3. Error bars indicate SD.
(G) Violin plot depicting the $\log_2$ FCs of all identified NF-κB target genes in CAL27 cells after HUWE1 or HAPSTR1 knockdown by three different siRNA target sequences each.
(H) Log_2 FCs of select NF-κB target genes in CAL27 cells after HUWE1 or HAPSTR1 knockdown. Each dot represents the mean of three replicates per siRNA used.
(I) 293T cells were transfected with siRNAs targeting the indicated genes followed by transfection with an NF-κB transcriptional reporter. Data are represented as the mean ± SD of four replicates. Statistical significance was determined by unpaired t test. ****$p \leq 0.0001$; **$p \leq 0.01$; n.s., $p > 0.05$.
(J) CAL27 cells were transfected with control or siRNAs targeting HUWE1 or HAPSTR1 in parental cells or cells with stable expression of the indicated siRNA-resistant HAPSTR1 variant. The abundance of *CCL20* and *CXCL3* mRNA in each sample normalized to that of *GAPDH* was determined by qRT-PCR analysis. Values in transgene-expressing cell lines were normalized to the control siRNA. Data are represented as the mean ± SEM of three biological replicates.
See also Figure S6 and Table S7.

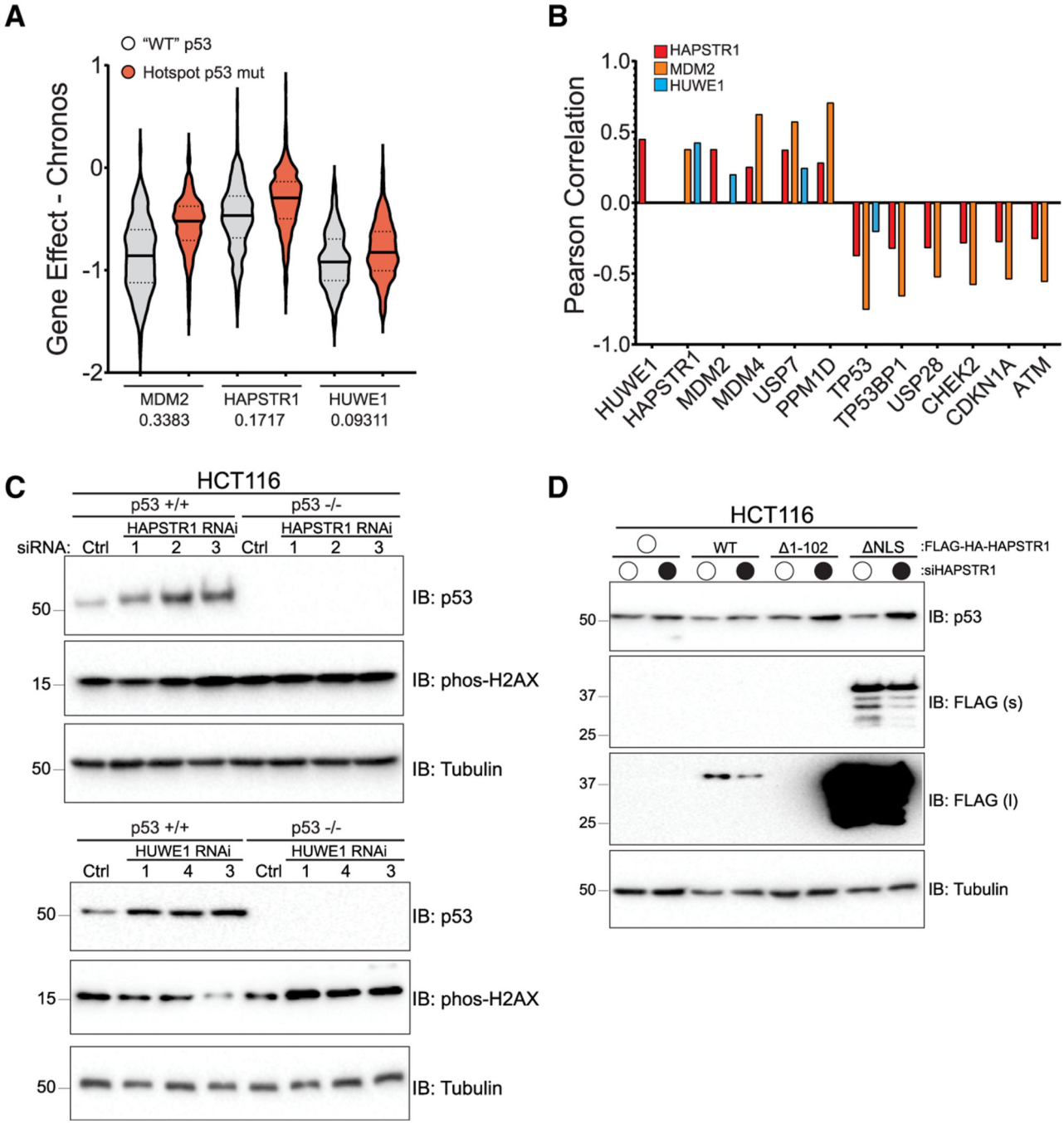

Figure 7. Loss of nuclear HUWE1 activates p53 signaling

(A) Violin plot of DepMap 22Q2 CRISPR gene effect scores for MDM2, HAPSTR1, and HUWE1 in cell lines with WT or hotspot mutations in p53. Numbers below gene name indicate mean difference comparing p53 WT or hotspot mutant cell lines.

(B) Pearson correlation values from DepMap 22Q2 CRISPR data comparing MDM2, HAPSTR1, and HUWE1 to the indicated p53 target gene or regulator.

(C) Immunoblots of HCT116 cells with the indicatedp53 status transfected with a control (Ctrl) siRNA or one of three siRNA sequences targeting HAPSTR1 (top) or HUWE1

(bottom). Whole-cell extracts were separated by SDS-PAGE and IB with the indicated antibodies.

(D) Immunoblots of HCT116 cells stably expressingthe indicated variant of siRNA-resistant FLAG-HA-tagged HAPSTR1 and transfected with a control or HAPSTR1-targeting siRNA. Whole-cell extracts were separated by SDS-PAGE and IB with the indicated antibodies. See also Figure S7.

KEY RESOURCES TABLE

REAGENT or RESOURCE	SOURCE	IDENTIFIER
Antibodies		
Mouse monoclonal anti-FLAG, Clone M2	Sigma-Aldrich	Cat#F3165; RRID:AB_259529
Rabbit polyclonal anti-REDD1 (DDIT4)	Proteintech	Cat#10638–1-AP; RRID:AB_2245711
Mouse monoclonal anti-Ubiquitin, clone Ubi-1	Millipore	Cat#MAB1510; RRID:AB_2180556
Rabbit polyclonal anti-sequestosome-1 (p62)	Bethyl Laboratories, Inc	Cat#A302–857A; RRID:AB_10631598
Mouse monoclonal anti-α-tubulin (DM1A)	Cell Signaling Technology	Cat#3873; RRID:AB_1904178
Rabbit polyclonal anti-Lasu1/Ureb1 (HUWE1)	Bethyl Laboratories, Inc	Cat#A300–486A; RRID:AB_2264590
Rabbit polyclonal anti-MAFB	Cell Signaling Technology	Cat#41019; RRID:AB_2799192
Mouse monoclonal anti-GFP	Roche	Cat#11814460001; RRID:AB_390913
Mouse monoclonal anti-p53 (DO-1)	Santa Cruz Biotechnology, Inc.	Cat#sc-126; RRID:AB_628082
Rabbit monoclonal anti-Phospho-Histone H2A.X (Ser139) (20E3)	Cell Signaling Technology	Cat#9718; RRID:AB_2118009
anti-Strep antibody HRP conjugate	Millipore	Cat#71591–3; RRID: AB_10806716
Rabbit polyclonal anti-Histone H3	Cell Signaling Technology	Cat#9715; RRID:AB_331563
Rabbit polyclonal anti-C16orf72 (HAPSTR1)	Aviva Systems Biology	Cat#ARP78805_P050
Mouse monoclonal anti-Phospho-p53 (S15) (16G8)	Cell Signaling Technology	Cat#9286; RRID:AB_331741
Rabbit monoclonal anti-Phospho-CHK1 (S345) (133D3)	Cell Signaling Technology	Cat#2348; RRID:AB_331212
Anti-Rabbit IgG (H + L), HRP Conjugate antibody	Promega	Cat#W4011; RRID:AB_430833
Anti-Mouse IgG (H + L), HRP Conjugate antibody	Promega	Cat#W4021; RRID:AB_430834
IRdye60 Anti-Mouse IgG secondary	LI-COR	Cat#926–68070; RRID: AB_10956588
Chemicals, peptides, and recombinant proteins		
Lipofectamine RNAiMax	Thermo Fisher	Cat#13778030
Lipofectamine 2000	Thermo Fisher	Cat#11668019
Lipofectamine 3000	Thermo Fisher	Cat#L3000001
TransIT-293	Mirus Bio LLC	Cat#MIR 2700
Protease inhibitor cocktail tablet	Roche	Cat#11836170001
Clarity Western ECL Substrate	BioRad	Cat#170–5061
Amersham ECL Prime	GE Life Sciences	Cat#RPN2232
MG132	Enzo Life Sciences	Cat#BML-PI102
Bafilomycin A1	Sigma	Cat#B1793
Doxycycline hydrochloride	Fisher Scientific	Cat#BP2653–5
TAK-243	ChemieTek	Cat#CT-M7243
Etoposide	Enzo	Cat#BML-GR307
Cisplatin	Enzo	Cat#ALX-400–040
Fetal bovine serum	VWR	Cat#97068–085
Trypsin	Sigma-Aldrich	Cat#T1426
N-Ethylmaleimide (NEM)	Sigma-Aldrich	Cat#E3876
Puromycin	Mediatech (Corning)	Cat#61–385-RA

REAGENT or RESOURCE	SOURCE	IDENTIFIER
Blasticidin S HCl	Corning	Cat#MT30100RB
Trizol	Life Technologies	Cat#1596026
Super-Script III First-Strand Synthesis System	Life Technologies	Cat#18080051
iTaq SYBR Green	Bio-Rad	Cat#1725121
Triton X-100	Sigma-Aldrich	Cat#T8787
EDTA	Amersco	Cat#E177
UBE2D2	R&D Systems	Cat#E2–622-100
10x E3 Ligase Conjugation Buffer	R&D Systems	Cat#B-71
UBE1	R&D Systems	Cat#E-304–050
Ubiquitin	R&D Systems	Cat#U-100H-10M
Mg-ATP	R&D Systems	Cat#B-20
Hoechst 33342 (20mM)	Thermo Scientific	Cat#62249
Fluoromount-G	Southern Biotech	Cat#0100–01
Human TNF-α Recombinant Protein	Cell Signaling Technology	Cat#16769
Critical commercial assays		
BCA Protein Assay	Thermo Scientific (Pierce)	Cat#23225
Dual-Glo Luciferase Assay System	Promega	Cat#E2920
CellTiter-Glo 2.0 Cell Viability Assay	Promega	Cat# G9243
Deposited data		
293T shHUWE1 TMT proteomics raw data	This paper	PRIDE: PXD041590
HAP1 HUWE1 KO/KI TMT proteomics raw data	This paper	PRIDE: PXD041591
HUWE1/HAPSTR1 IP proteomics raw data	This paper	PRIDE: PXD041593
CAL27 siHUWE1 siHAPSTR1 timsTOF proteomics raw data	This paper	PRIDE: PXD041595
293T shHUWE1 RNA-seq raw data	This paper	Zenodo; https://doi.org/10.5281/zenodo.7831879
CAL27 siRNA Control RNA-seq raw data	This paper	Zenodo; https://doi.org/10.5281/zenodo.7839090
CAL27 siHUWE1 RNA-seq raw data	This paper	Zenodo; https://doi.org/10.5281/zenodo.7839096
CAL27 siHAPSTR1 RNA-seq raw data	This paper	Zenodo; https://doi.org/10.5281/zenodo.7839102
Experimental models: Cell lines		
293T	ATCC	Cat#CRL-3216; RRID:CVCL_0063
HCT116 WT	Gift from Wade Harper (Harvard Medical School)	N/A
HCT116 p53 −/−	Gift from Wade Harper (Harvard Medical School)	N/A
CAL27	ATCC	Cat#CRL-2095; RRID:CVCL_1107
HAP1	Johnson et al.[64]	N/A
HAP1 iCas9	Hundley et al.[43]	N/A
HAP1 HUWE1 KO clone 3	Hundley et al.[43]	N/A

REAGENT or RESOURCE	SOURCE	IDENTIFIER
HAP1 HUWE1 KO clone 5	Hundley et al.[43]	N/A
NCI-H2052	ATCC	Cat#CRL-5915; RRID:CVCL_1518
RPE1 hTERT	Gift from Wade Harper (Harvard Medical School)	N/A
293T inducible_shHUWE1–154	This paper	N/A
293T inducible_shHUWE1–158	This paper	N/A
293T inducible_shHUWE1–890	This paper	N/A
293T inducible_shHUWE1–891	This paper	N/A
293T inducible_shHUWE1–2	This paper	N/A
293T inducible_shHUWE1–3	This paper	N/A
293T inducible_shFF (firefly control)	This paper	N/A
293T FLAG-HA-HAPSTR1 (cJM316)	This paper	N/A
293T FLAG-HA-SCNM1 (cJM330)	This paper	N/A
HAP1 HUWE1 C4341S Knock-in	This paper	N/A
CAL27 FLAG-HA-HAPSTR1 (cJM324)	This paper	N/A
CAL27 FLAG-HA-SCNM1 (cJM339)	This paper	N/A
CAL27 FLAG-HA-NFIB (cJM343)	This paper	N/A
CAL27 FLAG-HA-MAFB (cJM348)	This paper	N/A
CAL27 FLAG-HA-ZCCHC17 (cJM345)	This paper	N/A
293T FLAG-HA-HAPSTR1 (HAPSTR1 siRNA #1 resistant) (cJM349)	This paper	N/A
293T FLAG-HA-HAPSTR1 Δ1–102 (HAPSTR1 siRNA #1 resistant) (cJM351)	This paper	N/A
293T FLAG-HA-HAPSTR1 ΔNLS (HAPSTR1 siRNA #1 resistant) (cJM353)	This paper	N/A
CAL27 GFP-SCNM1 (cJM358)	This paper	N/A
CAL27 GFP-SCNM1 FLAG-HA-HAPSTR1 (HAPSTR1 siRNA #1 resistant) (cJM355)	This paper	N/A
CAL27 GFP-SCNM1 FLAG-HA-HAPSTR1 Δ1–102 (HAPSTR1 siRNA #1 resistant) (cJM356)	This paper	N/A
CAL27 GFP-SCNM1 FLAG-HA-HAPSTR1 ΔNLS (HAPSTR1 siRNA #1 resistant) (cJM357)	This paper	N/A
CAL27 FLAG-HA-SCNM1 Δ1–24 (cJM368)	This paper	N/A
CAL27 inducible Cas9 sgControl	This paper	N/A
CAL27 inducible Cas9 sgHUWE1	This paper	N/A
CAL27 inducible Cas9 sgHAPSTR1	This paper	N/A
CAL27 inducible Cas9 sgHUWE1 sgHAPSTR1	This paper	N/A
CAL27 inducible Cas9 sgHAPSTR1 FLAG-HAPSTR1	This paper	N/A
CAL27 inducible Cas9 sgHAPSTR1 FLAG-HAPSTR1 Δ1–102	This paper	N/A
CAL27 inducible Cas9 sgHAPSTR1 FLAG-HAPSTR1 ΔNLS	This paper	N/A
CAL27 GFP	This paper	N/A
HCT116 FLAG-HA-HAPSTR1	This paper	N/A
HCT116 FLAG-HA-HAPSTR1 Δ1–102	This paper	N/A
HCT116 FLAG-HA-HAPSTR1 ΔNLS	This paper	N/A

REAGENT or RESOURCE	SOURCE	IDENTIFIER
CAL27 FLAG-HA-HAPSTR1 (HAPSTR1 siRNA #1 resistant) (cJM350)	This paper	N/A
CAL27 FLAG-HA-HAPSTR1 Δ1–102 (HAPSTR1 siRNA #1 resistant) (cJM352)	This paper	N/A
CAL27 GFP-SCNM1 FLAG-HA-HAPSTR1 ΔNLS (HAPSTR1 siRNA #1 resistant) (cJM354)	This paper	N/A
Expi293F	Thermo-Fisher	Cat#A14635
Sf9	Expression Systems	Cat#94–001F
Hi5	Thermo-Fisher	Cat#B85502
Oligonucleotides		
siRNA targeting sequence: HUWE1_D-007185–01 (siHUWE1_1): GCAAAGAAAUGGAUAUCAA	Dharmacon	Cat#D-007185–01
siRNA targeting sequence: HUWE1 (siHUWE1_2): UGGUAGAUGUCCUUCAGAUUU	Dharmacon	N/A
siRNA targeting sequence: HUWE1 (siHUWE1_3): CACCUCAGCUACUUCAAGUUU	Dharmacon	N/A
siRNA targeting sequence: HUWE1_D-007185–06 (siHUWE1_4): GAAAUGGAUAUCAAACGUA	Dharmacon	Cat#D-007185–06
siRNA targeting sequence: HAPSTR1_D-031072–01 (siHAPSTR1_1): GGACAAUGGUGGAACUAGA	Dharmacon	Cat#D-031072–01
siRNA targeting sequence: HAPSTR1_D-031072–02 (siHAPSTR1_2): CAGAAGAACUAUUCGUCGA	Dharmacon	Cat#D-031072–02
siRNA targeting sequence: HAPSTR1_D-031072–04 (siHAPSTR1_3): GAUGUGUUGGCUUGGGUUA	Dharmacon	Cat#D-031072–04
siRNA targeting sequence: Non-targeting control siRNA pool #2	Dharmacon	Cat#D-001206–14
HUWE1 prime editing check forward: 5′-GTCCCTTCCTACAGATCCAGTG-3′	This paper	N/A
HUWE1 prime editing check reverse: 5′- CATCAAGTATGCAAGCTCAACC-3′	This paper	N/A
qRT-PCR Primers CCL20 forward: 5′-AACCATGTGCTGTACCAAGAG-3′	This paper	N/A
qRT-PCR Primers CCL20 reverse: 5′-CAGTCAAAGTTGCTTGCTTCTG-3′	This paper	N/A
qRT-PCR Primers CXCL3 forward: 5′-GCAGGGAATTCACCTCAAGA-3′	This paper	N/A
qRT-PCR Primers CXCL3 reverse: 5′-GTGTGGCTATGACTTCGGTT-3′	This paper	N/A
qRT-PCR Primers GAPDH forward: 5′-GGTGGTCTCCTCTGACTTCAACA-3′	This paper	N/A
qRT-PCR Primers GAPDH reverse: 5′-GTTGCTGTAGCCAAATTCGTTGT-3′	This paper	N/A
Recombinant DNA		
TRIPZ_shHUWE1_V2THS_353154	Dharmacon	Cat#RHS4696–200764225

REAGENT or RESOURCE	SOURCE	IDENTIFIER
TRIPZ_shHUWE1_V2THS_353155	Dharmacon	Cat#RHS4696–200765823
TRIPZ_shHUWE1_V2THS_353158	Dharmacon	Cat#RHS4696–200760498
TRIPZ_shHUWE1_V2THS_154890	Dharmacon	Cat#RHS4696–200698401
TRIPZ_shHUWE1_V2THS_154891	Dharmacon	Cat#RHS4696–200676399
TRIPZ_shHUWE1_V2THS_110969	Dharmacon	Cat#RHS4696–200673302
pIND_mirR_shFF	Meerbrey et al[65]	N/A
pDEST_pHAGE_N_FLAG-HA-HAPSTR1 (pJM336)	This paper	N/A
pDEST_pHAGE_N_FLAG-HA-SCNM1 (pJM416)	This paper	N/A
pDEST_pHAGE_N_FLAG-HA-NFIB (pJM426)	This paper	N/A
pDEST_pHAGE_N_FLAG-HA-MAFB (pJM417)	This paper	N/A
pDEST_pHAGE_N_FLAG-HA-ZCCHC17 (pJM427)	This paper	N/A
pDEST_pHAGE_N_FLAG-HA-HAPSTR1 siRNA#1resistant (pJM432)	This paper	N/A
pDEST_pHAGE_N_FLAG-HA-HAPSTR1 Δ1–102 siRNA#1resistant (pJM433)	This paper	N/A
pDEST_pHAGE_N_FLAG-HA-HAPSTR1 ΔNLS siRNA#1resistant (pJM434)	This paper	N/A
pDEST_pHAGE_N_GFP-SCNM1 (pJM435)	This paper	N/A
pDEST_pHAGE_N_FLAG-HA-SCNM1 Δ1–24 (pJM446)	This paper	N/A
pDEST_CMV_N_FLAG-MAFB (pJM420)	This paper	N/A
pDEST_CMV_N_FLAG-HUWE1 (WT) (pJM350)	Hunkeler et al.[13]	N/A
pDEST_CMV_N_FLAG-HUWE1 C4341S (CS) (pJM351)	This paper	N/A
pDEST_CMV_N_FLAG-HUWE1 Y1658A (Mut #2) (pJM369)	This paper	N/A
pDEST_CMV_N_FLAG-HUWE1 ΔBH3 (Mut #5) (pJM370)	This paper	N/A
pDEST_CMV_N_FLAG-HUWE1 ΔWWE (Mut #3) (pJM371)	This paper	N/A
pDEST_CMV_N_FLAG-HUWE1 BH3_4E (Mut #4) (pJM372)	Hunkeler et al.[13]	N/A
pDEST_CMV_N_FLAG-HUWE1 UBA_mut1 (Mut #8) (pJM375)	This paper	N/A
pDEST_CMV_N_FLAG-HUWE1 UBA_mut2 (Mut #9) (pJM376)	Hunkeler et al.[13]	N/A
pDEST_CMV_N_FLAG-HUWE1 UIM_mut (Mut #11) (pJM380)	Hunkeler et al.[13]	N/A
pDEST_CMV_N_FLAG-HUWE1 UBA-UIM_mut1 (Mut #13) (pJM381)	This paper	N/A
pDEST_CMV_N_FLAG-HUWE1 UBA-UIM_mut2 (Mut #14) (pJM382)	Hunkeler et al.[13]	N/A
pDEST_CMV_N_FLAG-HUWE1 Latch_L3294R (Mut #29) (pJM386)	This paper	N/A
pDEST_CMV_N_FLAG-HUWE1 Latch_L3294G (Mut #30) (pJM387)	This paper	N/A
pDEST_CMV_N_FLAG-HUWE1 Δ169–189 (Mut #19) (pJM388)	Hunkeler et al.[13]	N/A
pDEST_CMV_N_FLAG-HUWE1 F3194S (Mut #20) (pJM389)	Hunkeler et al.[13]	N/A

REAGENT or RESOURCE	SOURCE	IDENTIFIER
pDEST_CMV_N_FLAG-HUWE1 R110Q (Mut #21) (pJM390)	This paper	N/A
pDEST_CMV_N_FLAG-HUWE1 R4187C (Mut #23) (pJM391)	This paper	N/A
pDEST_CMV_N_FLAG-HUWE1 Δdisorder (Mut #24) (pJM392)	This paper	N/A
pDEST_CMV_N_FLAG-HUWE1 ΔTower (Mut #25) (pJM393)	This paper	N/A
pDEST_CMV_N_FLAG-HUWE1 UBA-UIM-UBM_mut (Mut #16) (pJM394)	Hunkeler et al.[13]	N/A
pDEST_CMV_N_FLAG-HUWE1 ΔUBA-UIM-UBM1 (Mut #17) (pJM395)	This paper	N/A
pDEST_CMV_N_FLAG-HUWE1 H669Q (Mut #22) (pJM399)	This paper	N/A
pDEST_CMV_N_FLAG-HUWE1 ΔPlug (Mut #31) (pJM400)	Hunkeler et al.[13]	N/A
pDEST_CMV_N_FLAG-HUWE1 Δ60 (Mut #32) (pJM401)	This paper	N/A
pDEST_CMV_N_FLAG-HUWE1 ΔUBA-UIM-3xUBM (Mut #18) (pJM419)	This paper	N/A
pNTM2_Flag_HAPSTR1 (pMH297)	This paper	N/A
pDEST_CMV_N_GFP_HAPSTR1 (pJM316)	This paper	N/A
pDEST_CMV_N_GFP-HAPSTR1 Δ1–102 siRNA#1resistant (pJM441)	This paper	N/A
pDEST_CMV_N_GFP-HAPSTR1 ΔNLS siRNA#1resistant (pJM442)	This paper	N/A
pDEST_CMV_N_GFP-MAFB (pJM437)	This paper	N/A
pCW-Cas9-Blast	Addgene	#83481
pHAGE_N_GFP_IRES-Blast Lenti (EJB466)	This paper	N/A
LentiGuide_Puro_sgPITCH/Control (pXG66)	This paper	N/A
LentiGuide_Puro_sgHAPSTR1 (pXG63)	This paper	N/A
LentiGuide_Puro_sgHUWE1 (pXG65)	This paper	N/A
LentiGuide_Puro_sgHAPSTR1_sgHUWE1 (pXG80)	This paper	N/A
pHAGE_CMV_N_FLAG_HA_HAPSTR1_WT_IRES_mCherry (EJB3991)	This paper	N/A
pHAGE_CMV_N_FLAG_HA_HAPSTR1 ΔNLS_IRES_mCherry (EJB3992)	This paper	N/A
pHAGE_CMV_N_FLAG_HA_HAPSTR1 Δ1–102_IRES_mCherry (EJB3990)	This paper	N/A
pSI-Check2-hRluc-NFkB-firefly	Addgene	#106979
PE2–2A-GFP	Addgene	#132776
pegRNA Huwe1 C4341S (pXG51)	This paper	N/A
pDARMO_CMVT_N_Strep_HUWE1_WT (pMH426)	This paper	N/A
pDARMO_CMVT_N_FLAG_SCNM1 (pMH539)	This paper	N/A
pAC8RedNK_Strep_HAPSTR1 (pMH255)	This paper	N/A
pDARMO_CMVT_N_Strep_HAPSTR1_1–251 (ΔNLS) (pMH541)	This paper	N/A
Software and algorithms		

REAGENT or RESOURCE	SOURCE	IDENTIFIER
FlowJo	BD Biosciences	N/A
Prism	GraphPad Software	N/A
CellProfiler	www.cellprofiler.org	N/A